Electronic Supplementary Information

A high tap density perovskite $NaTaO_3$ nanocrystal anode driven by pseudocapacitive conversion/intercalation hybrid mechanisms for advanced Li-ion/dual-ion storage

Tong Yan,[a] Rui Ding,[a]* Danfeng Ying,[a] Yongfa Huang,[a] Yuxi Huang,[a] Caini Tan,[a] Xiujuan Sun,[a] Ping Gao [a] and Enhui Liu[a]

[a]Key Laboratory of Environmentally Friendly Chemistry and Applications of Ministry of Education, College of Chemistry, Xiangtan University, Xiangtan, Hunan 411105, P.R. China

*E-mails: drm8122@163.com; drm8122@xtu.edu.cn

Table of contents

Experimental section

Synthesis of materials

The chemicals in the experiment were of analytical grade (A.R.) and directly used without further treatment (**Table S1**). The NTO sample was synthesized by using a hydrothermal strategy similar to the literature.[1-3] The compounds of 0.001 mol Ta_2O_5 and certain amounts of NaOH (0.5/8/10 M) were added into 35 mL deionized water, and dispersed well in an ultrasonic bath for 15 min under 100 W power conditions. Secondly, the mixture was transferred into a 50 mL Teflon-lined stainless-steel autoclave, which was heated in an electric oven (160 ℃, 12 h), and then cooled down naturally. Next, the yielded precipitates were collected by centrifugal filtration along with the washing with deionized water and absolute alcohol in sequence, and finally dried overnight at 100 ℃ to obtain the products.

Characterizations

The phases and crystalline properties were established by X-ray diffraction (XRD). The surface structures were verified by X-ray photoelectron spectra (XPS). The morphology and size of the particles were analyzed by scanning electron microscopy (SEM) and transmission electron microscopy (TEM). The crystalline microstructures were resolved by high-resolution TEM (HRTEM) and selected area electron diffraction (SAED). The elemental composition and distribution were measured by X-ray energy dispersive spectra (EDS) and mapping.

Electrochemical measurements

The electrodes were prepared by the following two steps: firstly, a well-dispersed mixture of 70 wt% active materials (as-synthesized NTO or commercial activated carbon (AC)/$LiFePO_4$/(LFP)/graphite(SAG/KS6), 15 wt% acetylene black (AB)/5 wt% superconductive carbon black conductive reagent, and 10 wt% polyvinylidene fluoride binder (PVDF, which was dissolved in N-methyl-2-pyrrolidone (NMP)) were cast onto the current collectors (Cu foil and carbon-coated Al foil were used as the collectors for the anode and cathode respectively, and the thickness was 15μm), followed by drying in a vacuum oven at 110 ℃ for 12 h; secondly, the electrodes were punched into disks with a diameter of 12 mm, and the mass loading of active materials was about 1.2 mg cm^{-2}. The electrochemical performances were examined by cyclic voltammetry (CV) and galvanostatic charge-discharge (GCD) tests via CHI660E electrochemical working stations and Neware-CT-4008 testers. Tests for electrodes (NTO/SAG/AC/LFP/KS6) were conducted in half-cells by using the type 2032 coin cells with a certain working electrode (WE), a Li plate as both the counter electrode (CE) and reference electrode (RE), and one piece of glass fiber (GF) as the separator. Tests for LICs, LIBs and Li-DIBs were conducted via full-cells with type 2032 coin cells, with the equal mass ratio of active materials of anode and cathode, and the NTO/SAG anodes were pre-lithiated at 0.1 A g^{-1} for 4.5 cycles (**Fig. S5**) before the assembly. The electrolytes used for electrodes were 1 M $LiPF_6$/EC:EMC:DMC (1:1:1) /1% VC (LBC-305-01, CAPCHEM). All cell assemblies were performed in a high pure Ar-filled dry glove-box (MIKROUNA, O_2 and H_2O<0.1 ppm) and all tests were carried out at room temperature (about 25 ℃) except the assigned tests at low (-20 ℃) and high (40 ℃) temperatures (more details information about the abovementioned chemicals, reagents and materials can be seen in **Table S1**).

Calculations for C_m, E_m, P_m

The specific capacity (C_m, mAh g^{-1}), energy density ($E_{m,1}$, Wh kg^{-1}) for LICs, energy density ($E_{m,2}$, Wh kg^{-1}) for LIBs and Li-DIBs, and power density (P_m, kW kg^{-1}) of different energy storage devices are calculated according to the equations **S(1)**-**(4)**.

$C_m=Q_m/3.6=It/3.6m$ **S(1)**

$E_{m,1}=(C_m\Delta V)/2$ **S(2)**

$E_{m,2}=(C_m V)$ **S(3)**

$P_m=3.6E_m/t_d$ **S(4)**

Where m, Q_m, ΔV, V, I and t_d refer to the mass of active materials (g, for half cells, it means the mass of active materials of anode or cathode; for full-cells, it means the total masses of active materials of anode and cathode), specific charge or discharge quantity (C g^{-1}, for anode, it means the charge quantity; for cathode and full-cells, it refers to the discharge quantity), voltage window (V), voltage of the discharging plateaus (V), current (A) and discharging time (s), respectively.

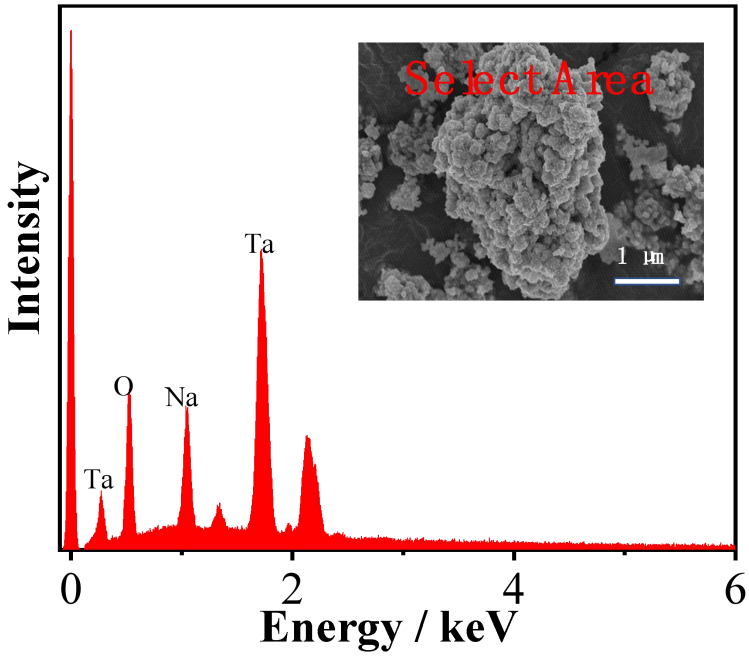

Fig. S1 The EDS data of the NTO sample .

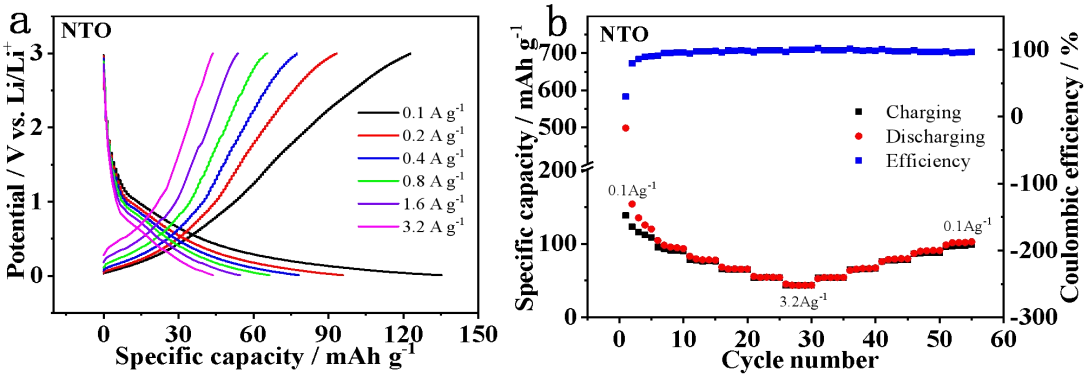

Fig. S2 GCD curves at 0.1-3.2 A g^{-1} (a), rate capability and coulombic efficiency at 0.1-3.2 A g^{-1} (b) of the NTO electrode.

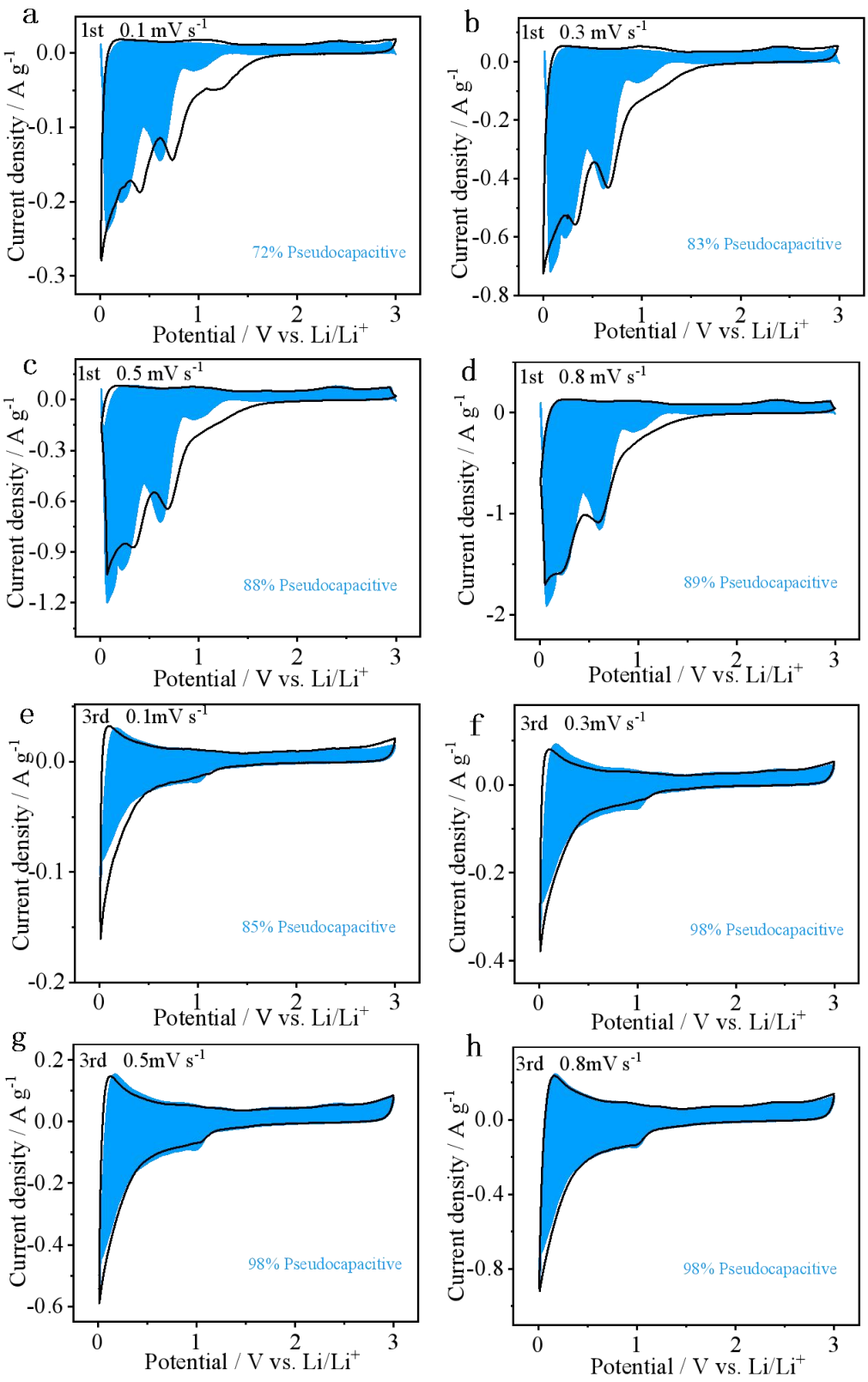

Fig. S3 The pseudocapacitive and diffusion-controlled contributions to charge storage in the NTO electrode (the shaded region is the identified pseudocapacitive contribution).

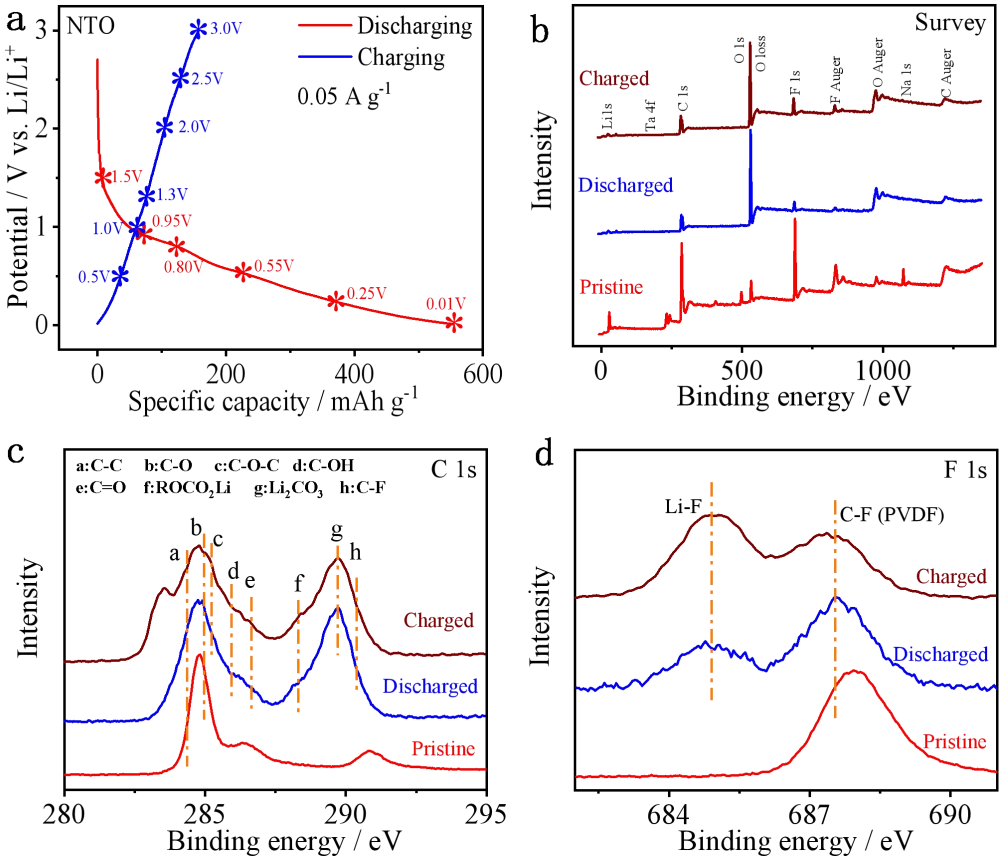

Fig. S4 The selected voltage states during the first cycle of GCD curves at 0.05 A g^{-1} (a), Ex situ XPS for survey (b), C1s (c) and F1s (d) in pristine and fully discharged/charged states of the NTO electrode.

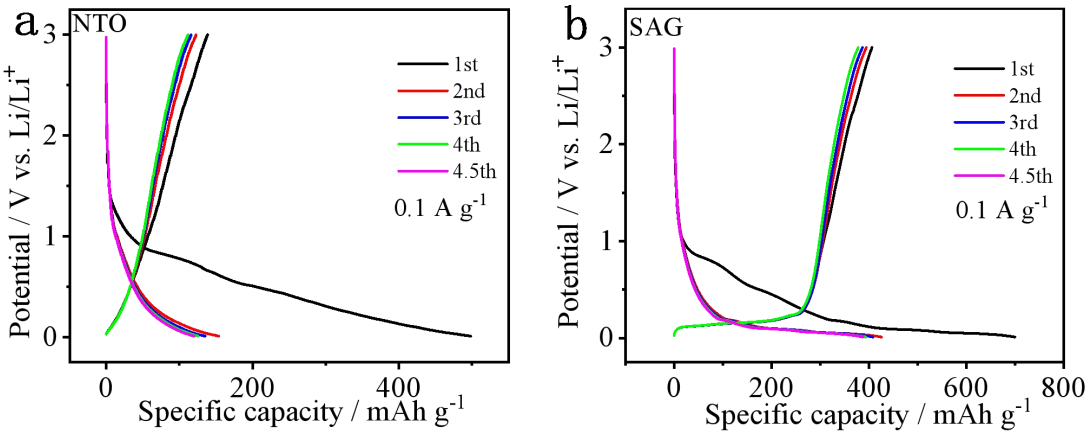

Fig. S5 The pre-charged (pre-lithiated) GCD plots at 0.1 A g^{-1} for 4.5 cycles of the NTO (a) and SAG (b) electrode.

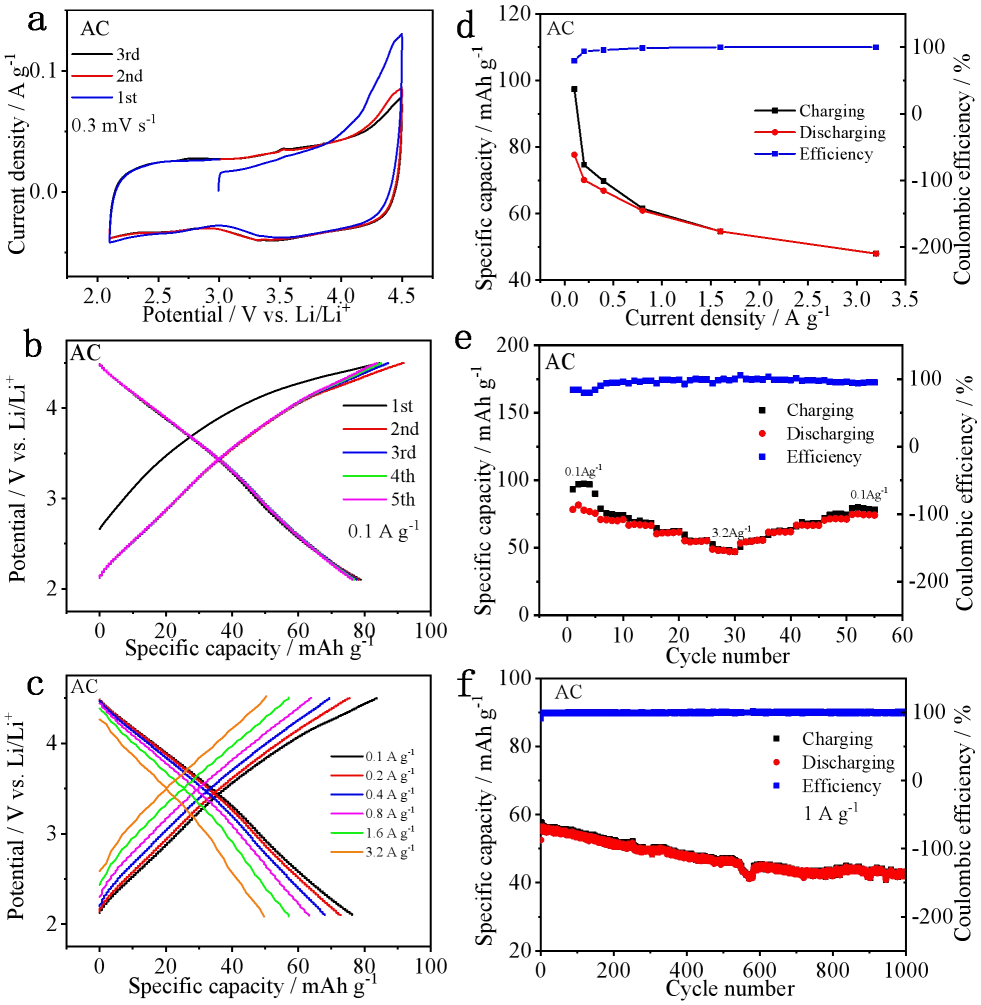

Fig. S6 Performance of the AC electrode: CV plots at 0.3 mV s^{-1} (a); GCD curves at 0.1 A g^{-1} (b) and 0.1 A g^{-1}-3.2 A g^{-1} (c); specific capacity, rate capability and coulombic efficiency at 0.1-3.2 A g^{-1} (d, e); cycling behavior at 1 A g^{-1} (f).

Activated carbon (AC) was chosen as the positive electrode for the construction of the NTO//AC LICs. **Fig. S6**a-c show the CV plots at 0.3 mV s^{-1} and GCD curves at 0.1 A g^{-1} and 0.1-3.2 A g^{-1} within a potential window of 2.1-4.5 V, which show the basically a rectangular CV shape and the linear GCD curve, revealing that the AC electrode is operated by a characteristic non-Faradaic capacitive reaction. The adsorption/desorption of ions on the surface of the AC electrode occur in the charge/discharge processes, indicating the typical electric double layer (EDL) behavior and the superior electrochemical reversibility. The specific capacity, rate capability and cycling behavior are shown in **Fig. S6**d-f, showing that the AC electrode exhibits the specific capacity values of 78-48 mAh g^{-1} at 0.1-3.2 A g^{-1} and 81% retention for 1000 cycles at 1 A g^{-1} (**Table. S3**, ESI). Such exceptional performance of AC electrode can be a good cathode used in LICs.

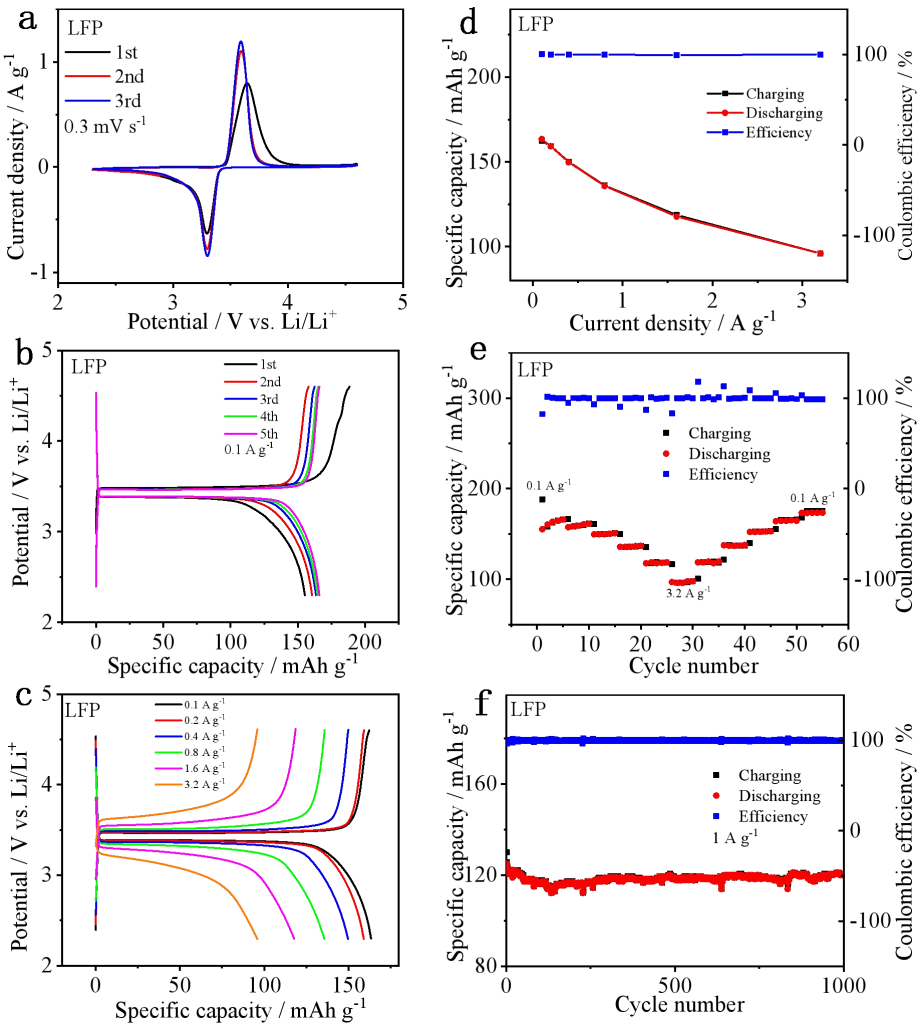

Fig. S7 Performance of the LFP electrode: CV plots at 0.3 mV s^{-1} (a); GCD curves at 0.1 A g^{-1} (b) and 0.1 A g^{-1}-3.2 A g^{-1} (c); specific capacity, rate capability and coulombic efficiency at 0.1-3.2 A g^{-1} (d, e); cycling behavior at 1 A g^{-1} (f).

$LiFePO_4$ (LFP) was chosen as the cathode for the construction of the NTO//LFP LIBs. **Fig. S7**a-c show the CV plots and GCD curves, which exhibits the typical Faradaic behavior of a battery electrode under the potential range of 2.3-4.6 V, showing the typical redox peaks or the charing/discharging plateaus at about 3.6/3.3 V because of the Li-ion de-intercalation/interecalations. The specific capacity, rate capability and cycling behavior are shown in **Fig. S7**d-f, showing that the LFP electrode exhibits the specific capacity values of 163.4-96.0 mAh g^{-1} at 0.1-3.2 A g^{-1} and 96% retention for 1000 cycles at 1 A g^{-1} (**Table S3**, ESI). Such an excellent performance of LFP can be a good cathode material used in LIBs and will contribute to the advanced performance of the NTO//LFP LIBs.

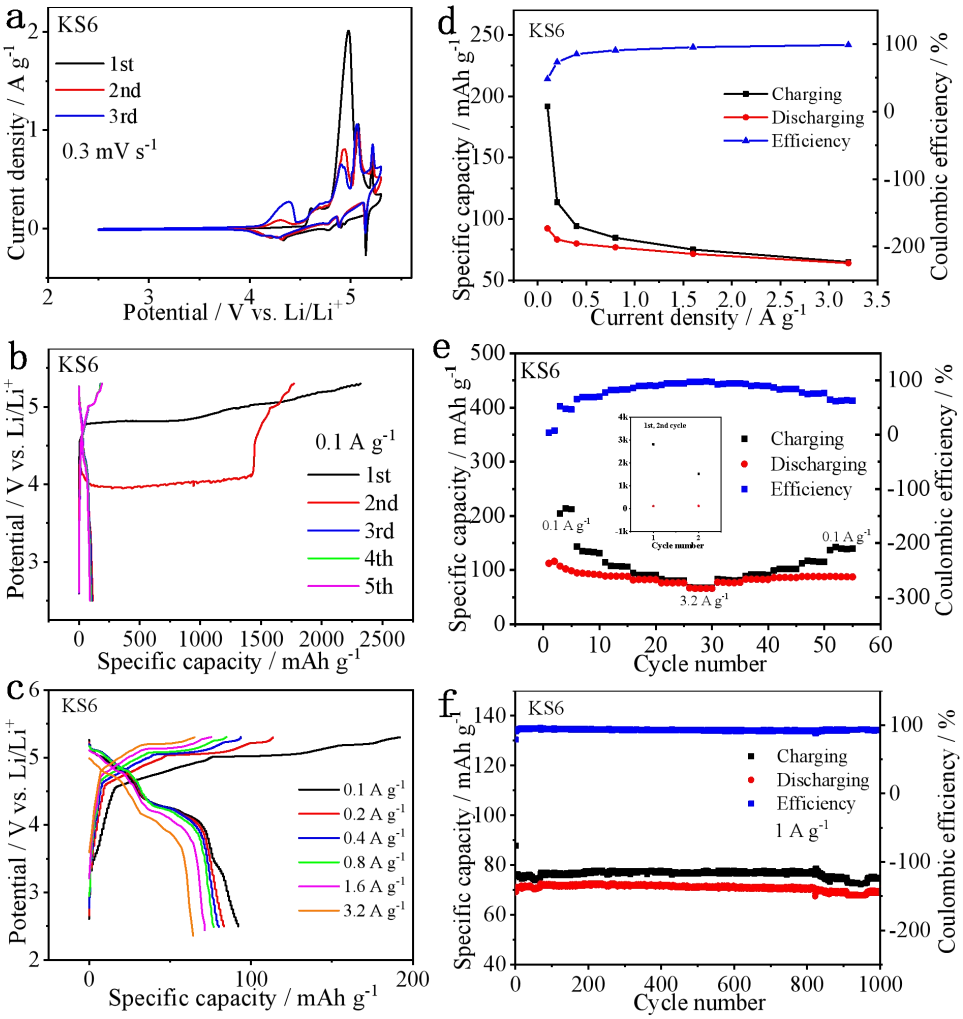

Fig. S8 Performance of the KS6 electrode:[4] CV plots at 0.3 mV s^{-1} (a); GCD curves at 0.1 A g^{-1} (b) and 0.1 A g^{-1}-3.2 A g^{-1} (c); specific capacity, rate capability and coulombic efficiency at 0.1-3.2 A g^{-1} (d, e); cycling behavior at 1 A g^{-1} (f).

Graphite (KS6) was chosen as the cathode for the construction of the NTO//KS6 Li-DIBs.[4] **Fig. S8**a-c show the CV plots and GCD curves, which show more than three pairs of redox peaks and charging/discharging plateaus in potential range of 2.5-5.3 V, suggesting the multi-steps co-insertions of PF_6^- anions and solvents in the graphite layers. Note that the charging specific capacity of the KS6 electrode for the first two cycles is so large, which may be owing to the highly irreversible kinetics (i.e. the intercalation rate is far faster than the corresponding de-intercalation rate) at the low charging rates. The specific capacity, rate capability and cycling behavior are shown in **Fig. S8**d-f, showing that the KS6 electrode exhibits the specific capacity values of 92-64 mAh g^{-1} at 0.1-3.2 A g^{-1} and 83% retention for 1000 cycles at 1 A g^{-1} (**Table S3**, ESI). Such an excellent performance of KS6 can be a good cathode material used in Li-DIBs and will contribute to the advanced performance of the NTO//KS6 Li-DIBs.

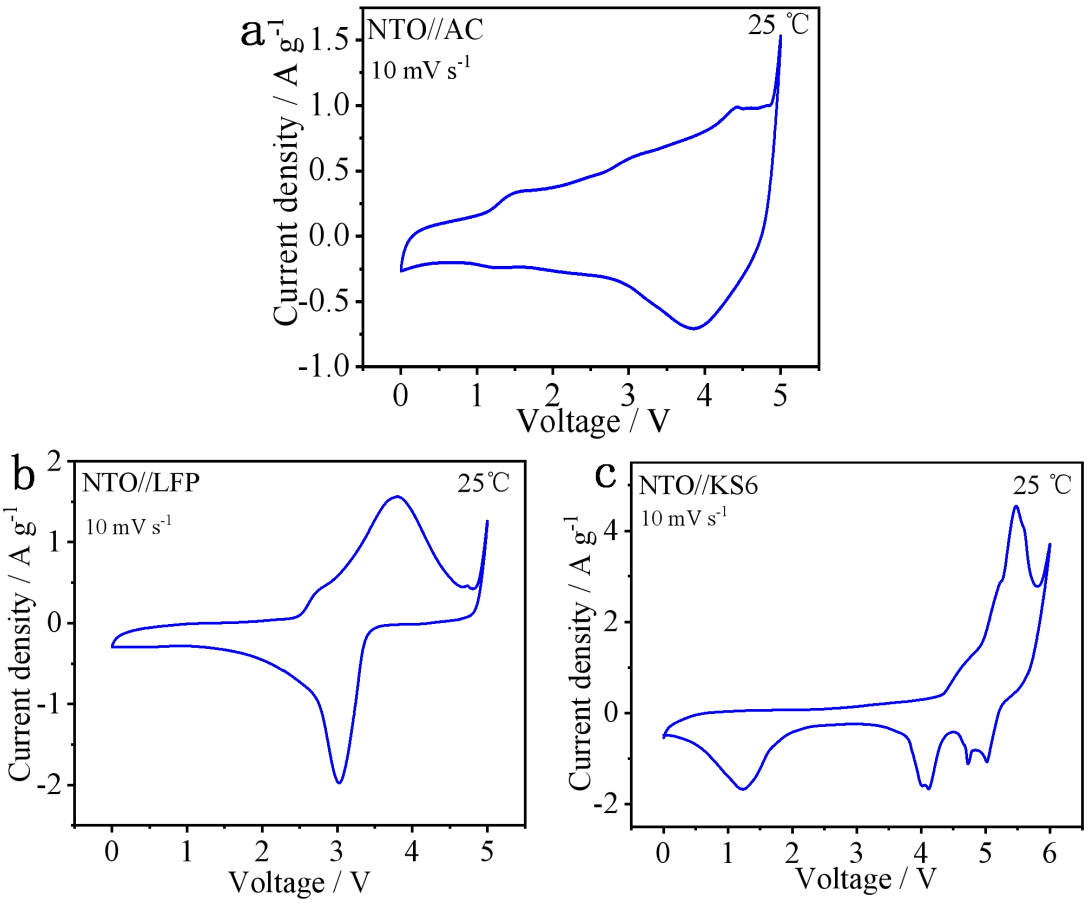

Fig. S9 The voltage windows of NTO//AC LICs (a), NTO//LFP LIBs (b) and NTO//KS6 Li-DIBs (c) at room temperatures (25°C).

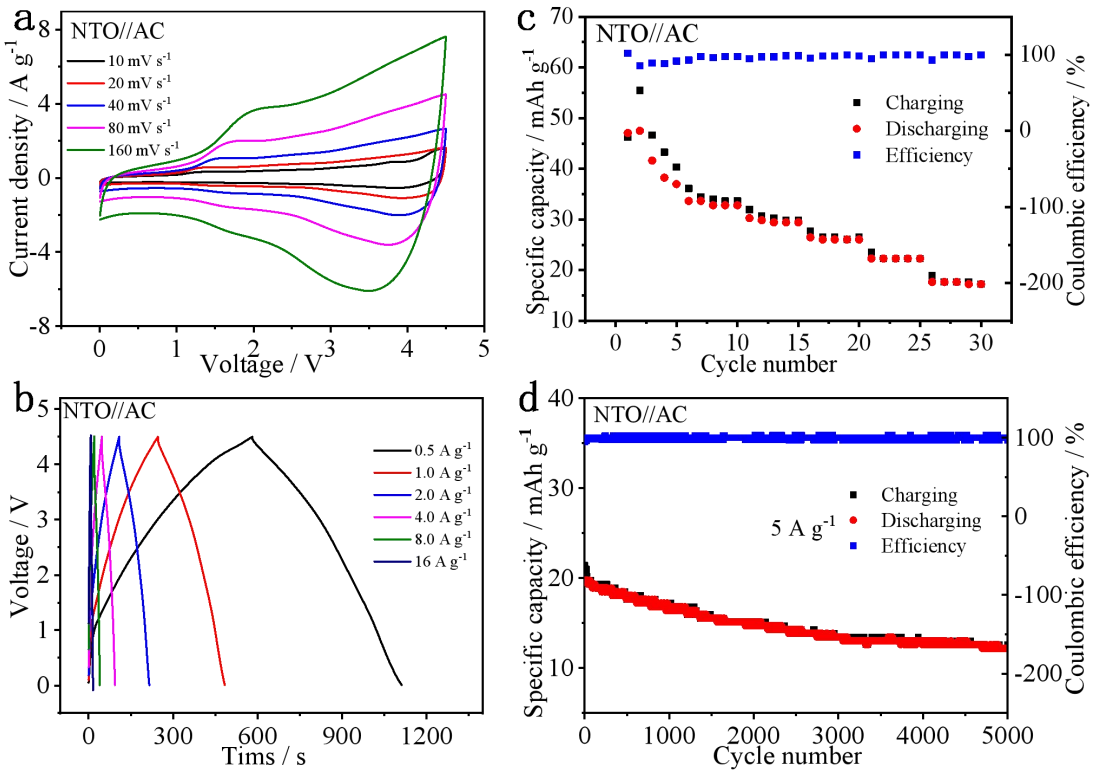

Fig. S10 The performance of NTO//AC LICs at room temperature: CV plots at 10-160 mV s^{-1} (a), GCD curves at 0.5-16 A g^{-1} (b), rate capability at 0.5-16 A g^{-1} (c) and cycling behavior at 5 A g^{-1} (d).

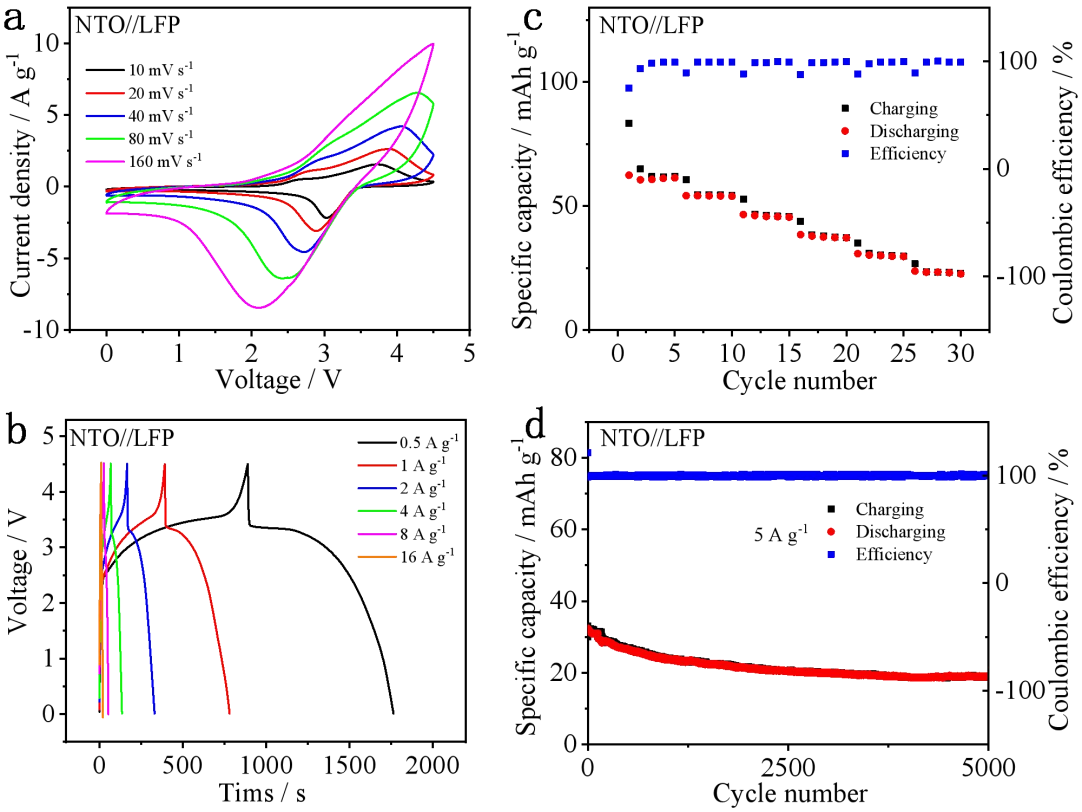

Fig. S11 The performance of NTO//LFP LIBs at room temperature: CV plots at 10-160 mV s^{-1} (a), GCD curves at 0.5-16 A g^{-1} (b), rate capability at 0.5-16 A g^{-1} (c) and cycling behavior at 5 A g^{-1} (d).

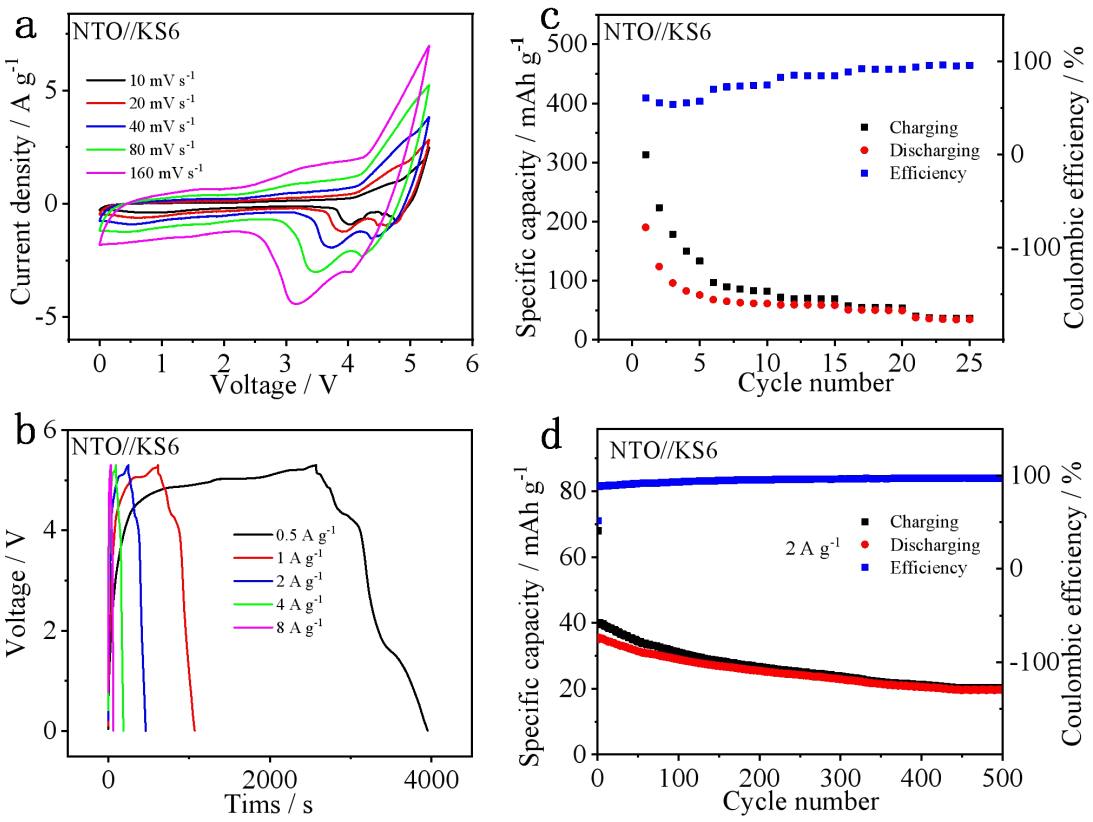

Fig. S12 The performance of NTO//KS6 Li-DIBs at room temperature: CV plots at 10-160 mV s^{-1} (a), GCD curves at 0.5-8 A g^{-1} (b), rate capability at 0.5-8 A g^{-1} (c) and cycling behavior at 2 A g^{-1} (d).

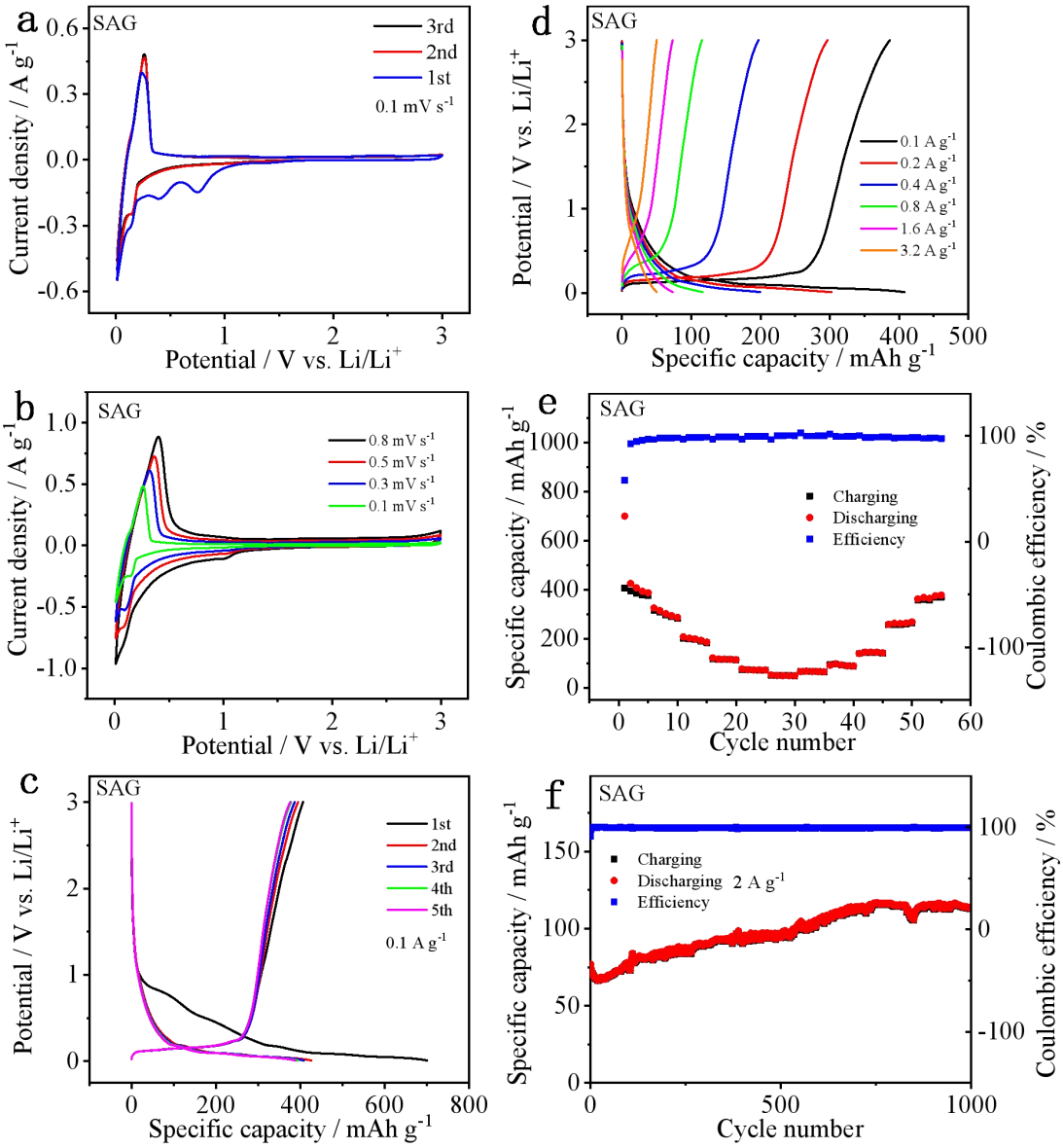

Fig. S13 Performance of the SAG electrode: CV plots for the first three cycles at 0.1 mV s^{-1} (a); the CV plots at the 0.1-0.8 mV s^{-1} of the third cycles (b); GCD curves at 0.1 A g^{-1} (c) and 0.1 A g^{-1}-3.2 A g^{-1} (d); rate capability and coulombic efficiency at 0.1-3.2 A g^{-1} (e); cycling behavior at 2 A g^{-1} (f).

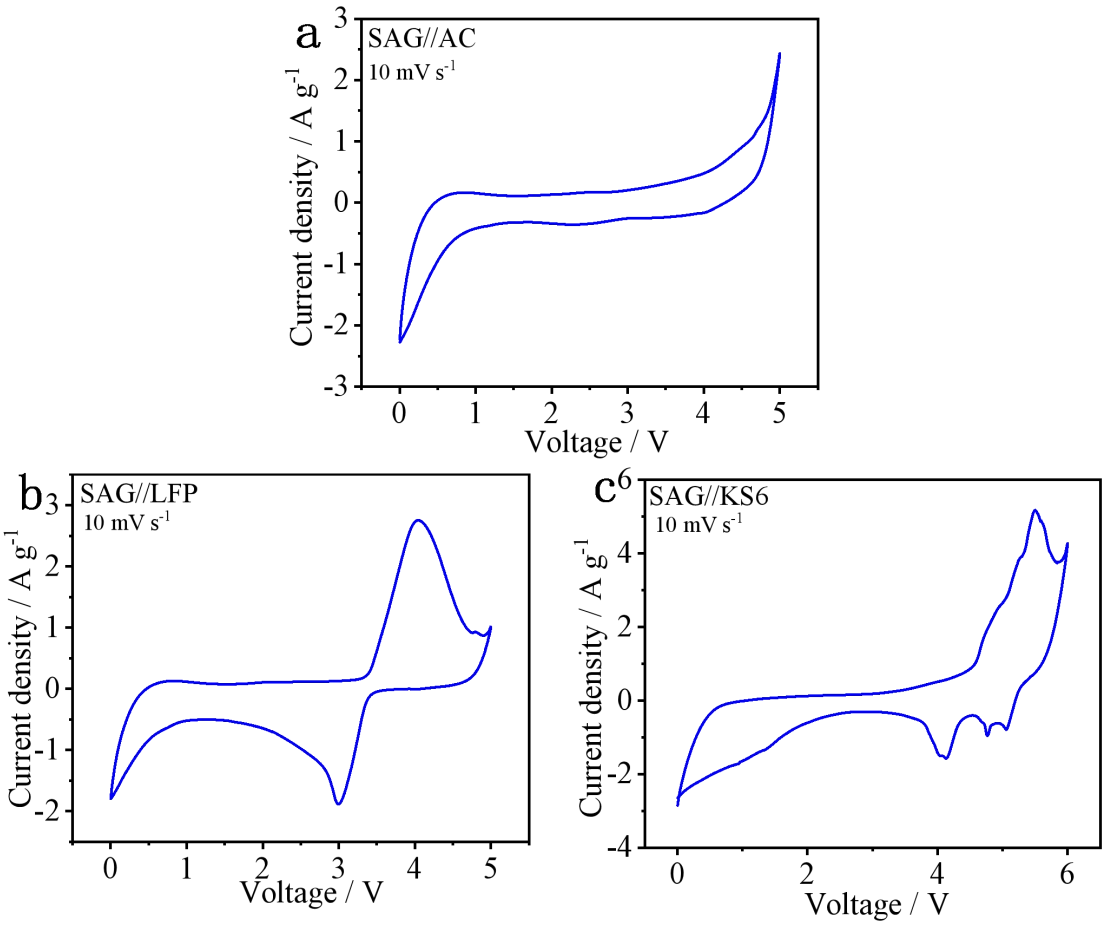

Fig. S14 The voltage windows of SAG//AC LICs (a), SAG//LFP LIBs (b) and SAG//KS6 Li-DIBs (c) at room temperature (25°C) .

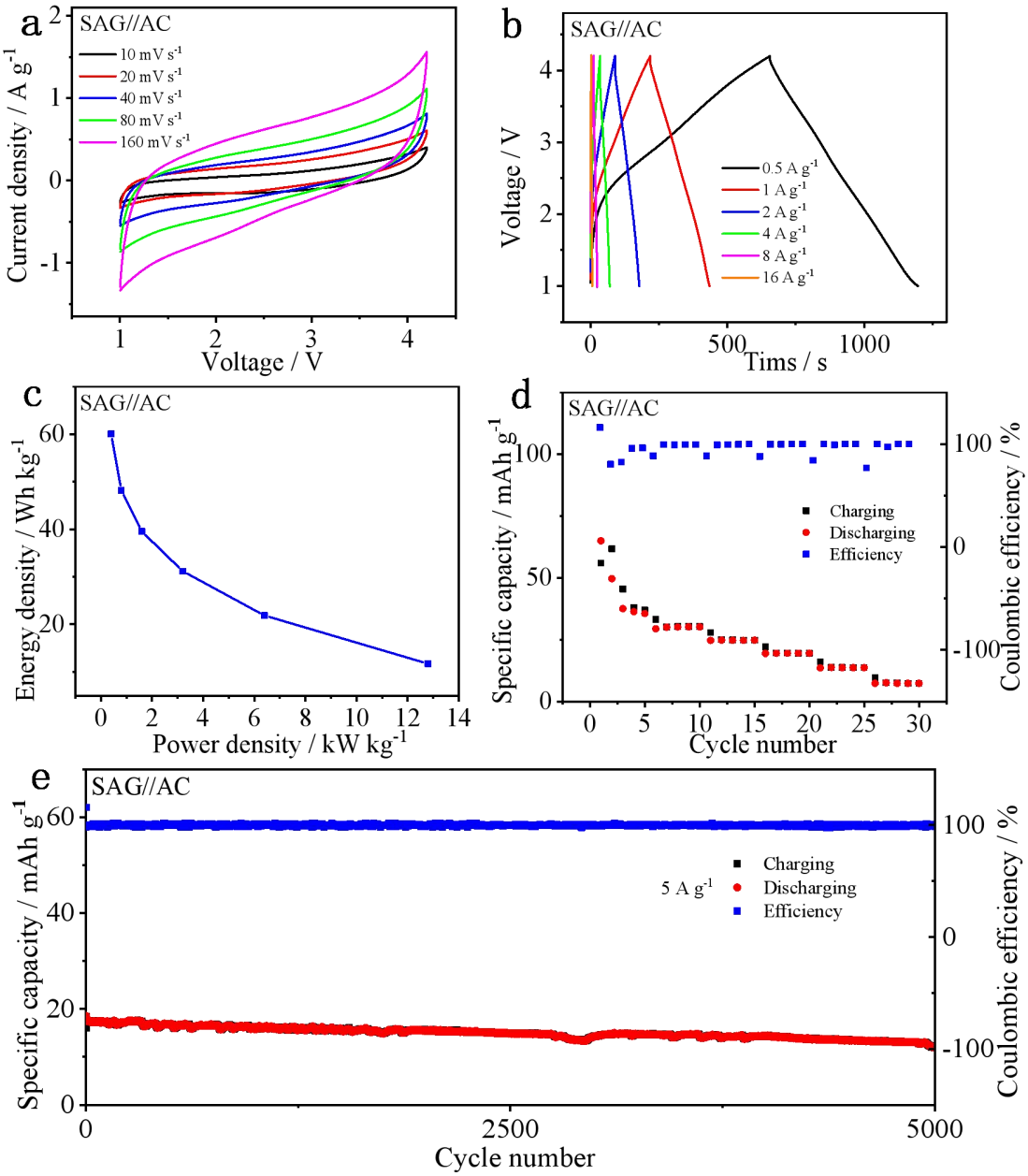

Fig. S15 The performance of SAG//AC LICs at room temperature: CV plots at 10-160 mV s^{-1} (a), GCD curves at 0.5-16 A g^{-1} (b), Ragone plots (c), rate capability at 0.5-16 A g^{-1} (d) and cycling behavior at 5 A g^{-1} (e) under the working voltages of 1.0-4.2 V.

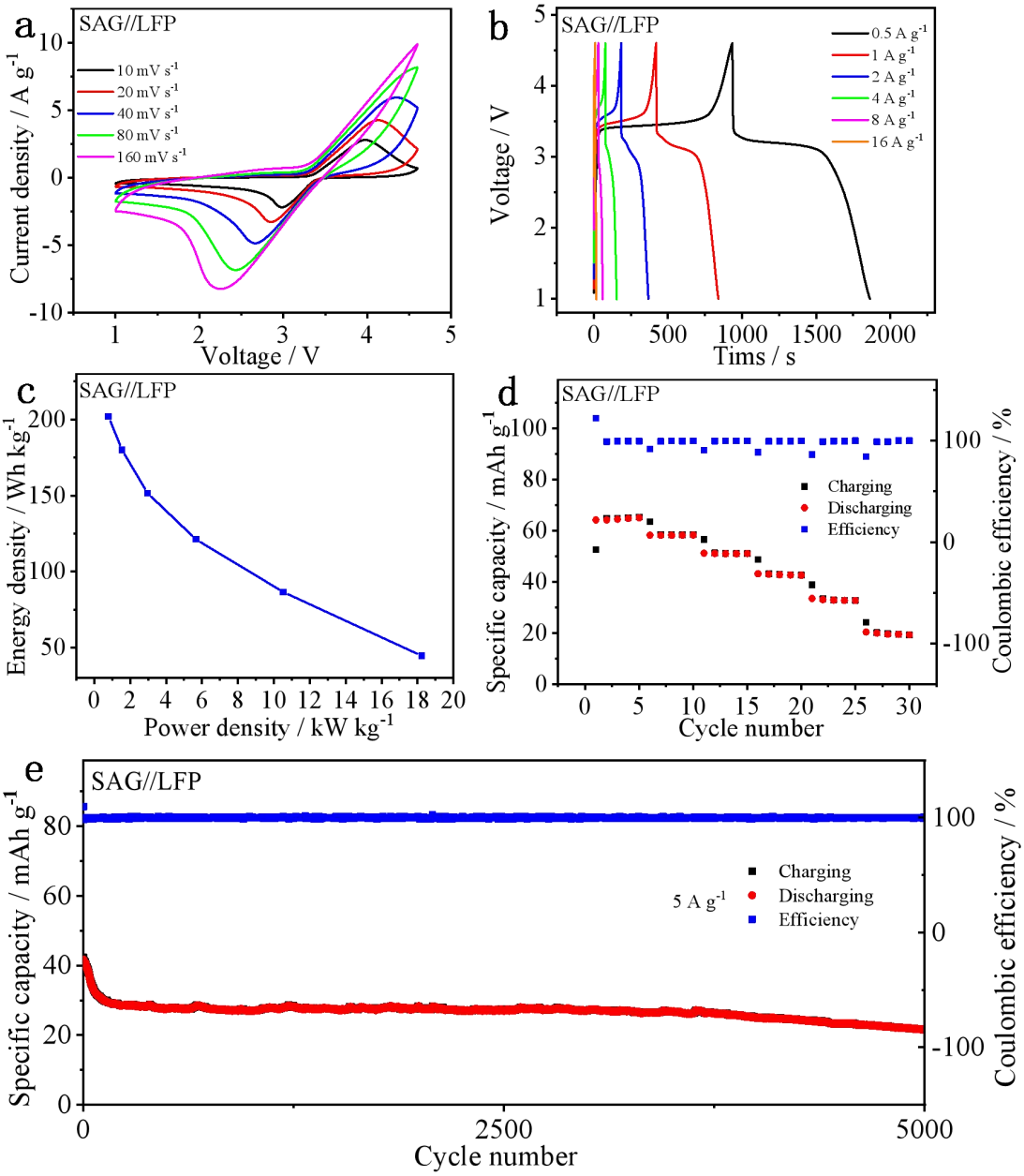

Fig. S16 The performance of SAG//LFP LIBs at room temperature: CV plots at 10-160 mV s^{-1} (a), GCD curves at 0.5-16 A g^{-1} (b), Ragone plots (c), rate capability at 0.5-16 A g^{-1} (d) and cycling behavior at 5 A g^{-1} (e) under the working voltages of 1.0-4.6 V.

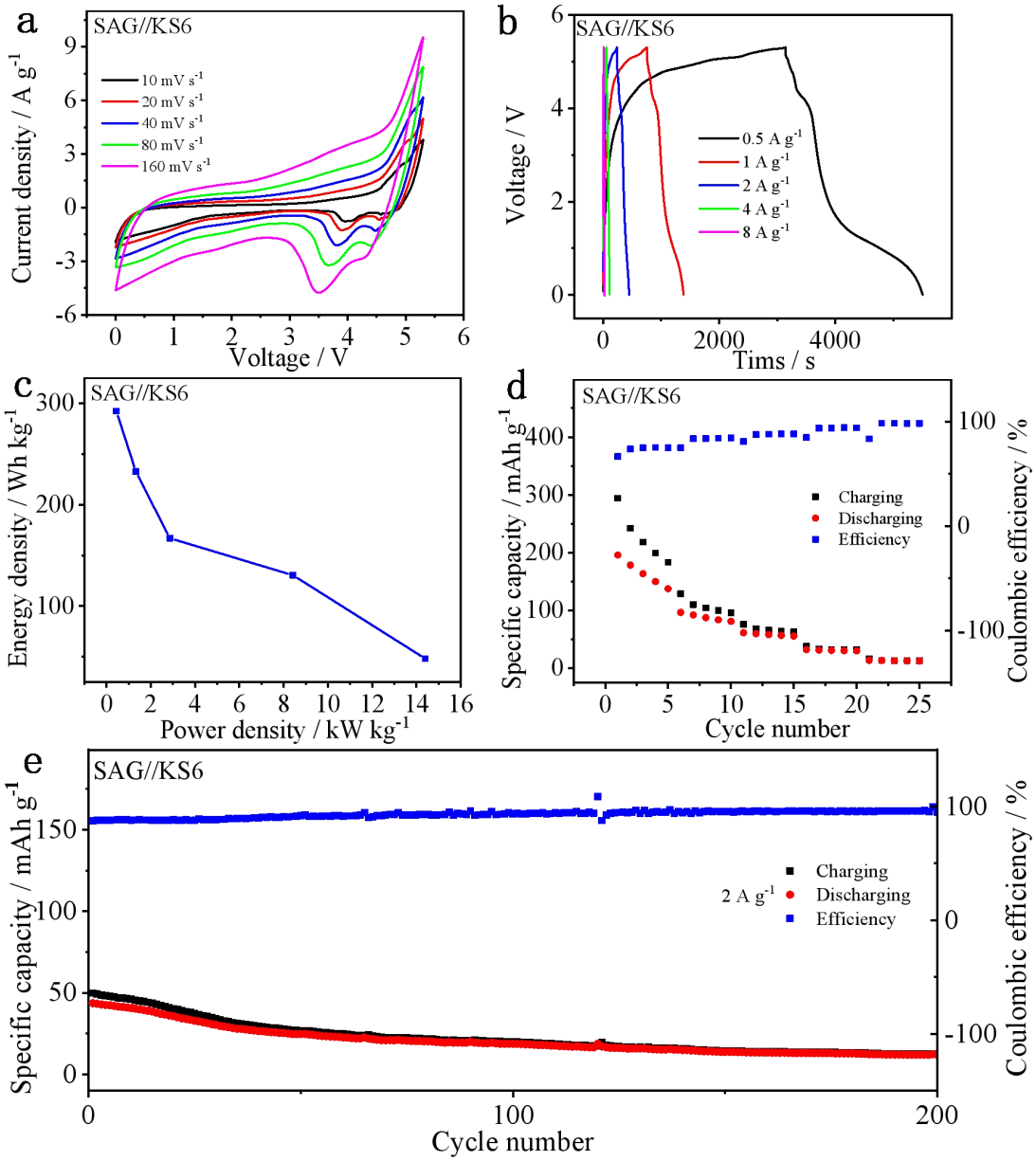

Fig. S17 The performance of SAG//KS6 Li-DIBs at room temperature: CV plots at 10-160 mV s^{-1} (a), GCD curves at 0.5-8 A g^{-1} (b), Ragone plots (c), rate capability at 0.5-8 A g^{-1} (d) and cycling behavior at 2 A g^{-1} (e) under the working voltages of 0.01-5.3 V.

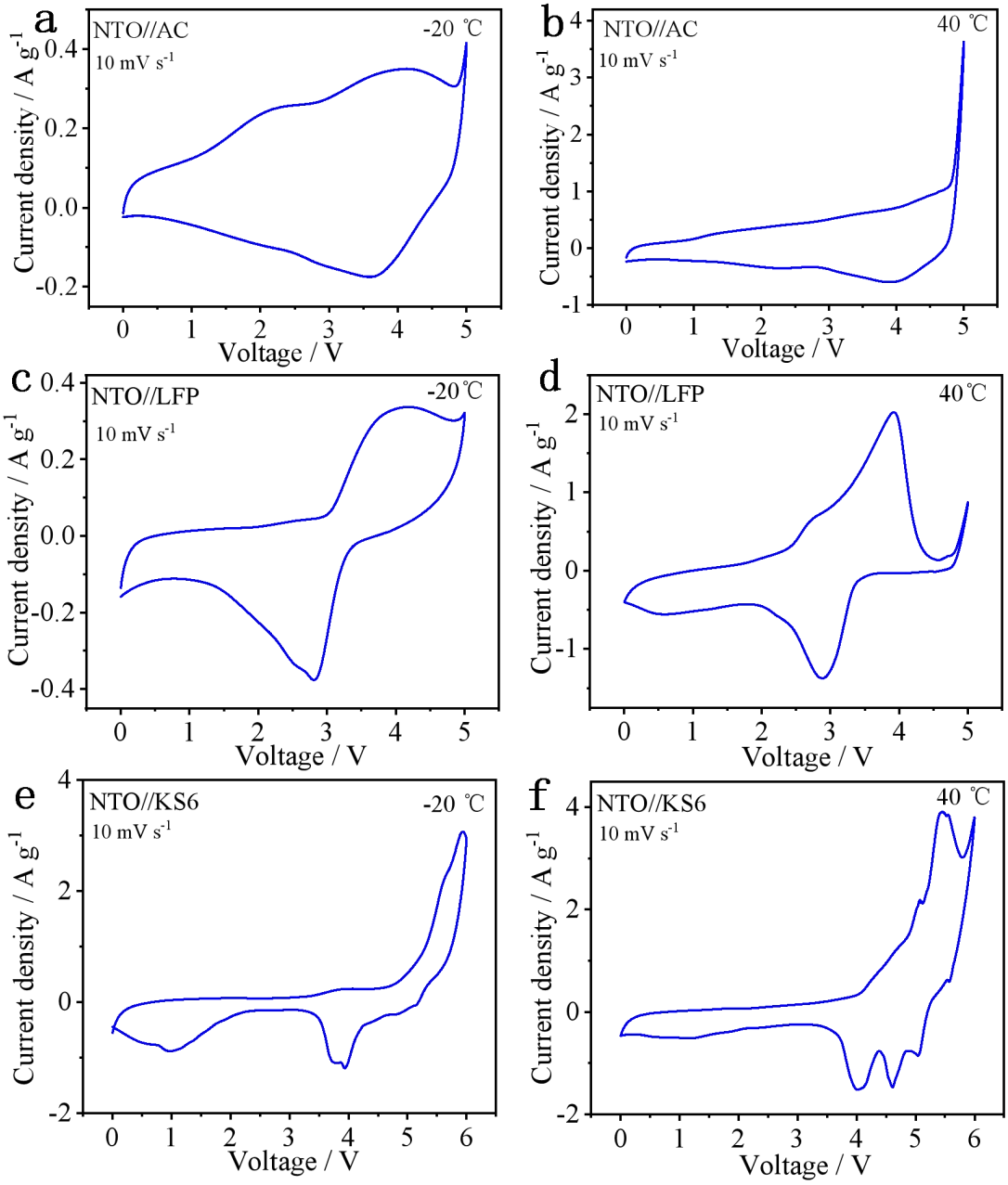

Fig. S18 The voltage windows of NTO//AC LICs (a, b), NTO//LFP LIBs (c, d) and NTO//KS6 Li-DIBs (e, f) at low (-20 °C) and high (40 °C) temperatures.

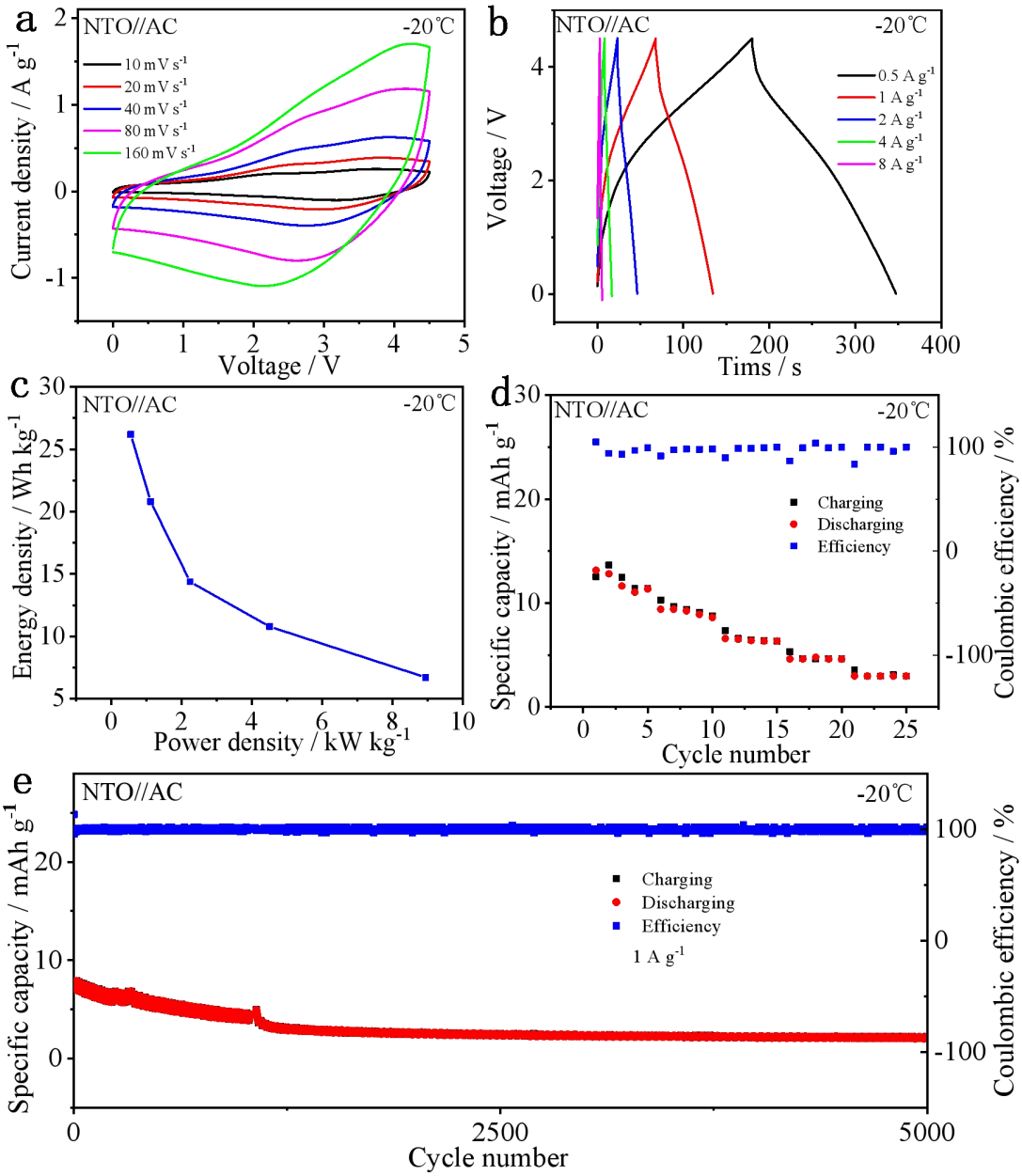

Fig. S19 The performance of NTO//AC LICs at low temperature (-20 °C): CV plots at 10-160 mV s^{-1} (a), GCD curves at 0.5-8 A g^{-1} (b), Ragone plots (c), rate capability at 0.5-8 A g^{-1} (d) and cycling behavior at 1 A g^{-1} (e).

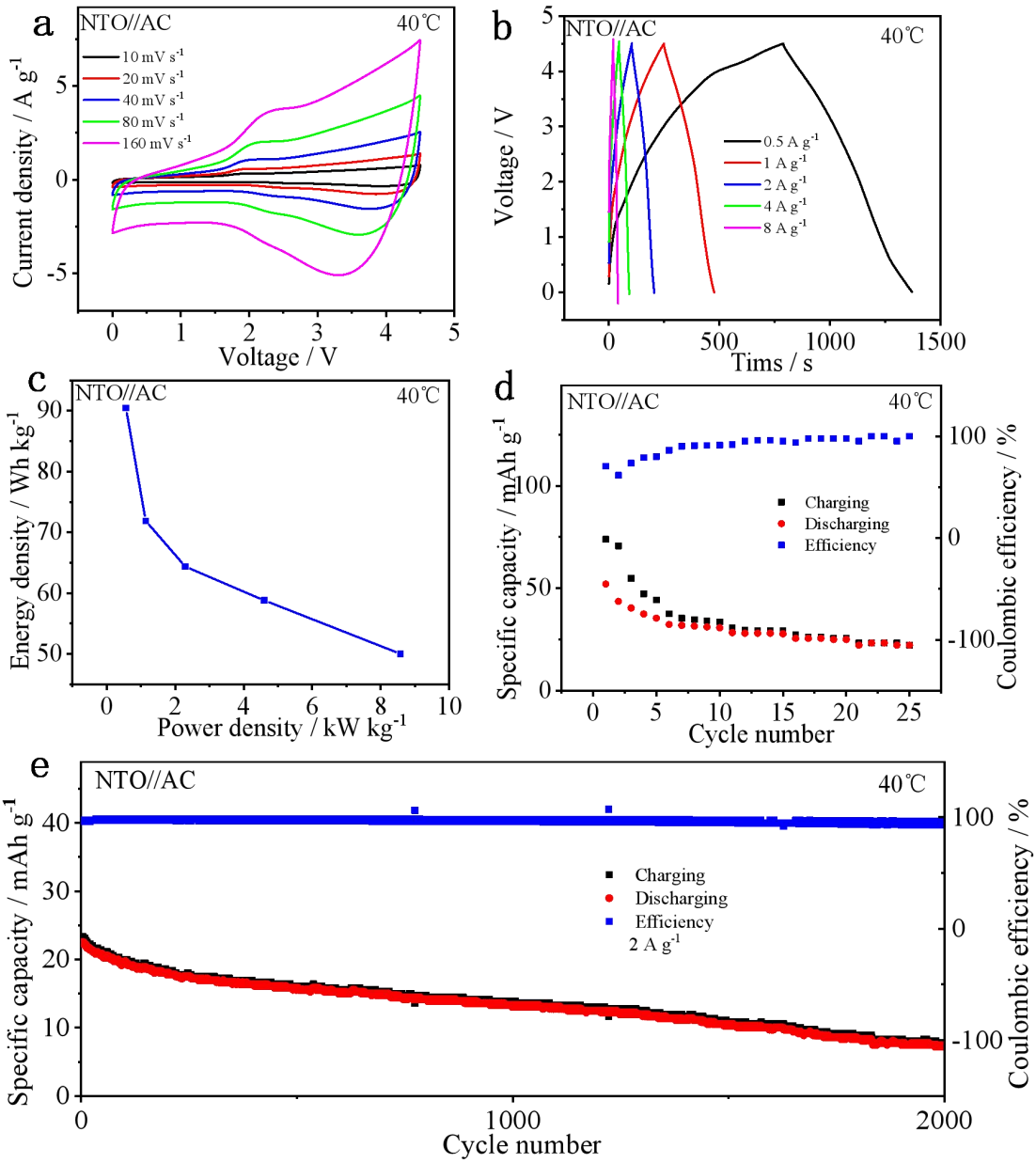

Fig. S20 The performance of NTO//AC LICs at high temperature (40 °C): CV plots at 10-160 mV s^{-1} (a), GCD curves at 0.5-8 A g^{-1} (b), Ragone plots (c), rate capability at 0.5-8 A g^{-1} (d) and cycling behavior at 2 A g^{-1} (e).

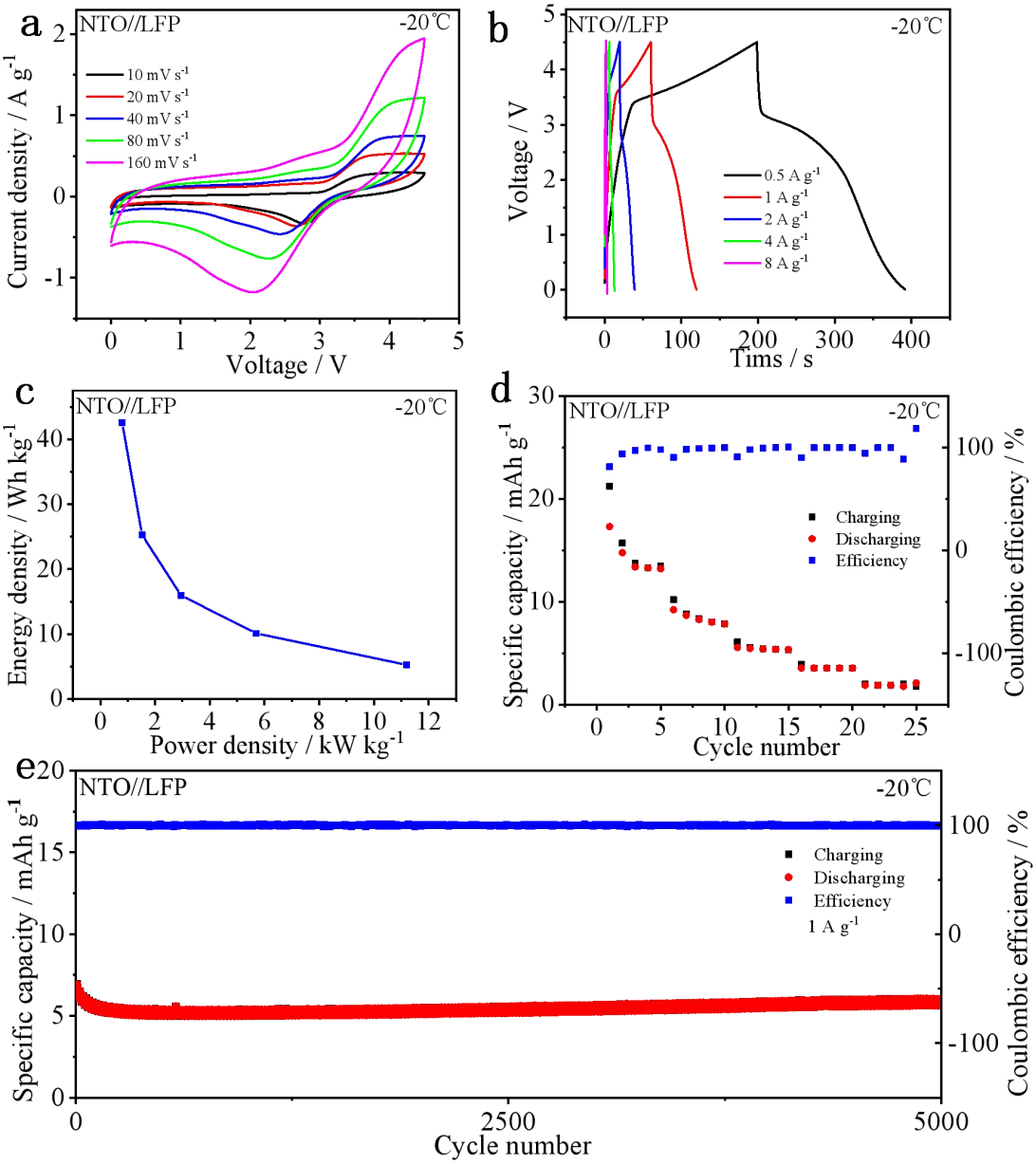

Fig. S21 The performance of NTO//LFP LIBs at low temperature (-20 °C): CV plots at 10-160 mV s^{-1} (a), GCD curves at 0.5-8 A g^{-1} (b), Ragone plots (c), rate capability at 0.5-8 A g^{-1} (d) and cycling behavior at 1 A g^{-1} (e).

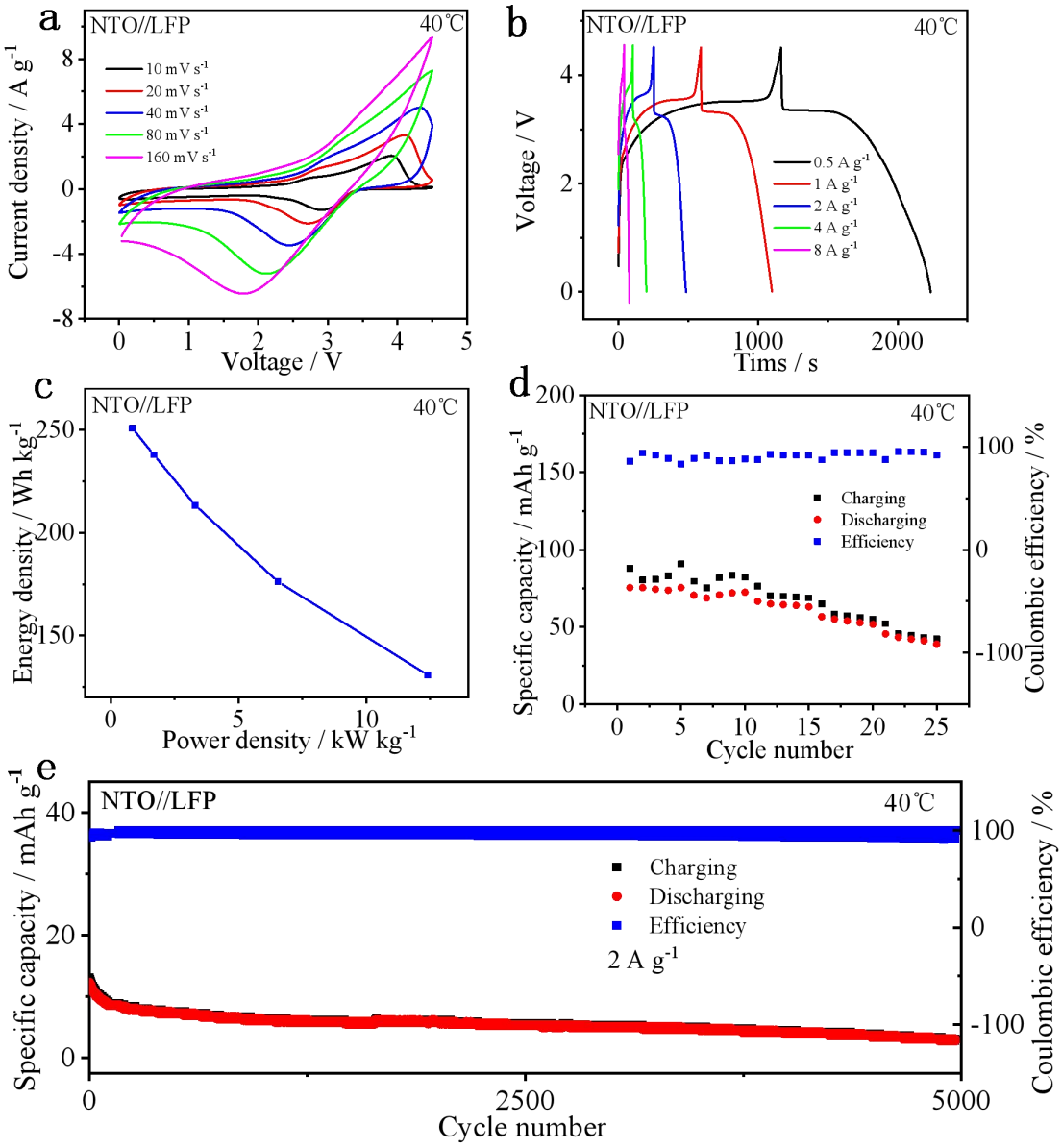

Fig. S22 The performance of NTO//LFP LIBs at high temperature (40 °C): CV plots at 10-160 mV s^{-1} (a), GCD curves at 0.5-8 A g^{-1} (b), Ragone plots (c), rate capability at 0.5-8 A g^{-1} (d) and cycling behavior at 2 A g^{-1} (e).

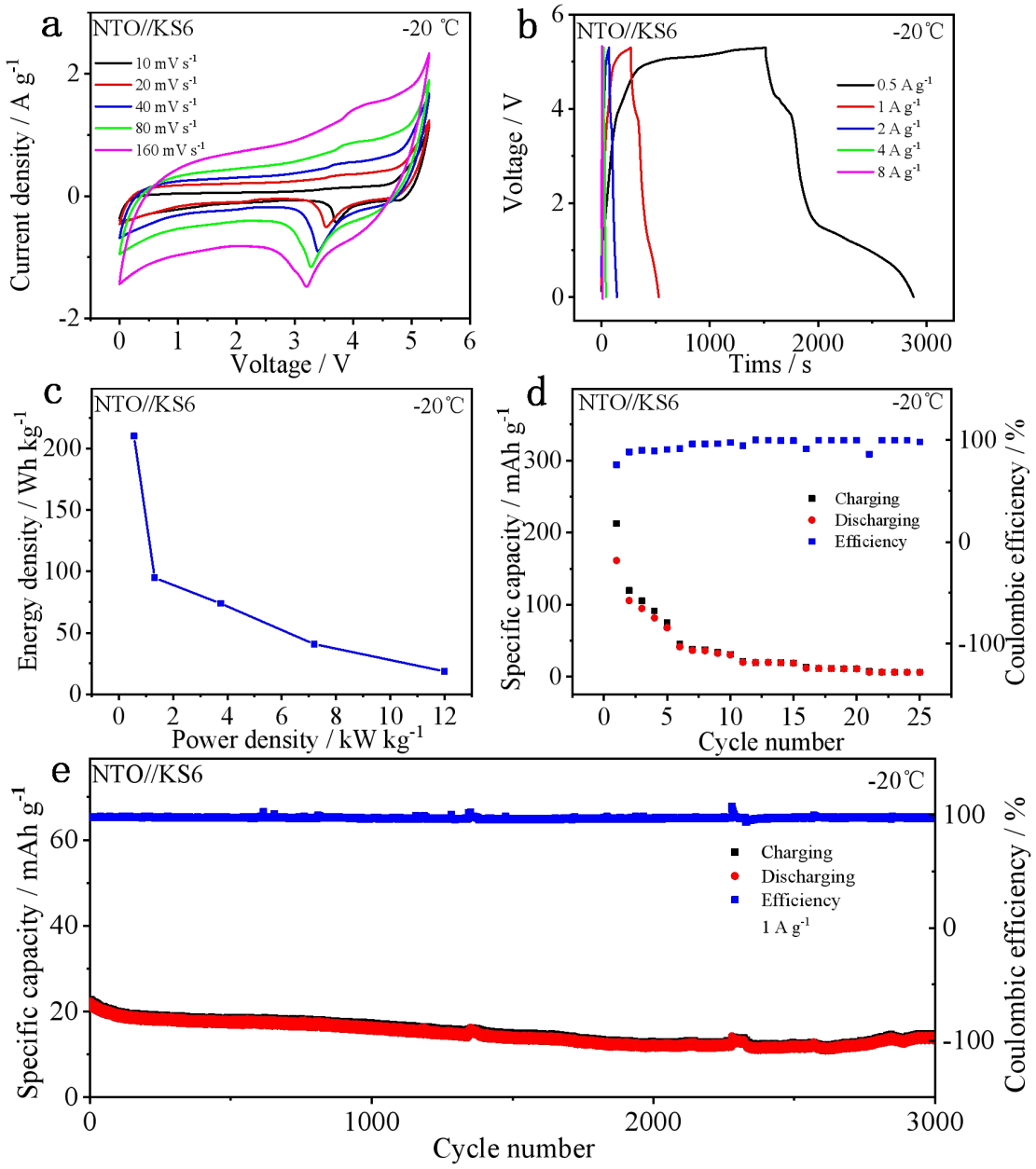

Fig. S23 The performance of NTO//KS6 Li-DIBs at low temperature (-20 °C): CV plots at 10-160 mV s^{-1} (a), GCD curves at 0.5-8 A g^{-1} (b), Ragone plots (c), rate capability at 0.5-8 A g^{-1} (d) and cycling behavior at 1 A g^{-1} (e).

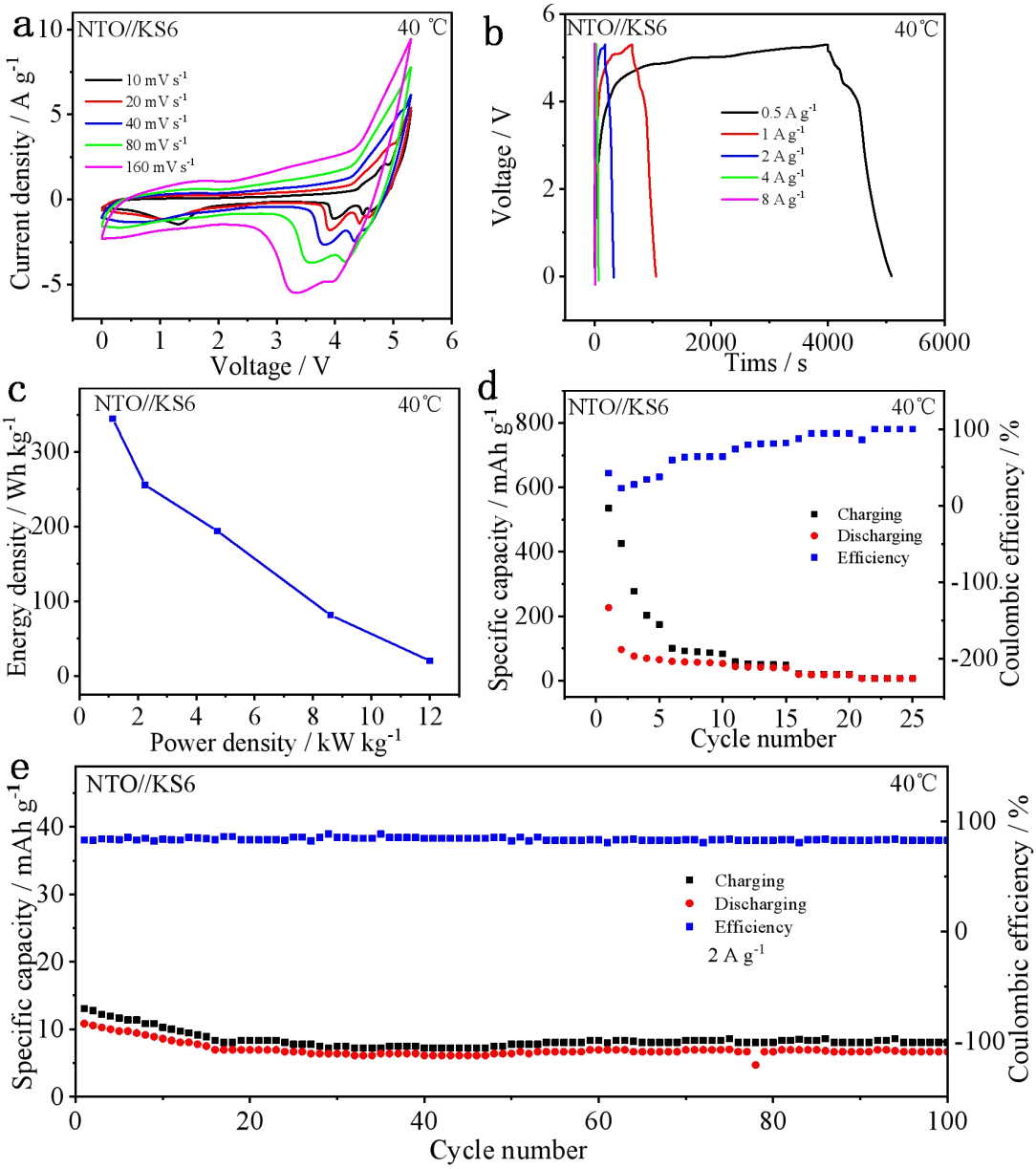

Fig. S24 The performance of NTO//KS6 Li-DIBs at high temperature (40 °C): CV plots at 10-160 mV s^{-1} (a), GCD curves at 0.5-8 A g^{-1} (b), Ragone plots (c), rate capability at 0.5-8 A g^{-1} (d) and cycling behavior at 2 A g^{-1} (e).

Table S1. Chemicals, reagents and materials used in the study.

Chemicals, Reagents and Materials	Type	Company	Characteristics
Ta_2O_5	AR	SinoPharm	purity≥99.99%
NaOH	AR	SinoPharm	purity≥96.0%
Activated carbon	YEC 8b	FuZhou YiHuan	D50: ~10 μm; Density: 0.4 g cm^{-3}; SSA:2000~2500 m^2 g^{-1}
$LiFePO_4$	LFP-NCO	Aleees	D50: 4 ± 2 μm; Tab: 1 ± 0.2 g cm^{-3}; SSA: 13 ± 2 m^2 g^{-1}
Graphite	KS6	TiMCAL	D90: 5.8-7.1 μm; Interlayer distance: 0.3354-0.3360 nm; SSA: 20 m^2 g^{-1}; Density-Scott: 0.07 g cm^{-3}
Graphite	SAG	BTR	D50: 19.0 ±1.5 μm; Tab: 0.9 ±0.1 g cm^{-3}; SSA:3.3 ± 0.5 m^2 g^{-1}
Superconductive carbon black	Battery grade	JH	/
AB	Battery grade	JH	/
NMP	AR	Kermel	purity≥99.0%
PVDF	Battery grade	JH	/
Electrolytes	LBC-305-01	CAPCHEM	1 M $LiPF_6$/EC:EMC:DMC (1:1:1) /1% VC
Li plate	15.6*0.45 mm	China Energy	15.6*0.45 mm
Cu foil	200*0.015	GuangZhou JiaYuan	Total thickness: 15 μm; weight: 87 g m^{-2}
Carbon coated-Al foil	222*0.015	GuagZhou NaNuo	Total thickness: 17 μm; Strength: 192 Mpa
Glass microfiber filters	GF/D 2.7 μm; 1823-025	Whatman	Diameter: 25 mm; Thickness: 675 μm; weight: 121 g m^{-2}
Cell components	CR-2032	ShenZhen TianChenHe	/

Table S2. Performance of the NTO/SAG electrodes.

Electrode	Specific capacity (mAh g^{-1}) at 0.1-3.2 A g^{-1}						Working voltage / V	Cycling behavior Retention% / 2 A g^{-1}/ 1000 cycles	Tap density / g cm^{-3}
	0.1	0.2	0.4	0.8	1.6	3.2			
NTO	**116.2**	**91.1**	**76.2**	**65.2**	**54.3**	**43.4**	**0.01-3.0**	**202%**	**2.53**
SAG	386.6	296	197	115	73.2	50.2	0.01-3.0	160%	0.9

Table S3. Performance of the AC/LFP/KS6 electrodes.

Electrode	Specific capacity (mAh g^{-1}) at 0.1-3.2 A g^{-1}						Working voltage / V	Cycling behavior Retention% / 1 A g^{-1} / 1000 cycles
	0.1	0.2	0.4	0.8	1.6	3.2		
AC	77.7	70.1	66.9	60.9	54.7	48.0	2.1-4.5	81%
LFP	163.4	159.2	150.2	135.8	118.1	96.0	2.3-4.6	96%
KS6	92.1	83.3	80.2	77.1	72.2	64.0	2.5-5.3	83%

Table S4. Performance summary of the LICs, LIBs and Li-DIBs in the study under room temperature (25 °C).

Type	Cell system	Working voltage / V	Energy density / Wh kg^{-1}	Power density / kW kg^{-1}	Cycling behavior / retention%, repeated cycles, current density
LICs	**NTO//AC**	**0.01-4.5**	**88.4-75.5** **69.1-61.1** **52.2-43.4**	**0.7-1.1** **2.3-4.5** **8.9-18.2**	**80%/1000/5 A g^{-1}** **72%/2000/5 A g^{-1}** **66%/3000/5 A g^{-1}** **64%/4000/5 A g^{-1}** **63%/5000/5 A g^{-1}**
	SAG//AC	1.0-4.2	60.0-48.1 39.5-31.2 21.8-11.5	0.4-0.8 1.6-3.2 6.4-12.8	84%/1000/5 A g^{-1} 82%/2000/5 A g^{-1} 76%/3000/5 A g^{-1} 76%/4000/5 A g^{-1} 63%/5000/5 A g^{-1}
LIBs	**NTO//LFP**	**0.01-4.5**	**205-182** **151-119** **92-70**	**0.9-1.7** **3.3-6.3** **12.3-24.1**	**80%/1000/5 A g^{-1}** **71%/2000/5 A g^{-1}** **67%/3000/5 A g^{-1}** **63%/4000/5 A g^{-1}** **60%/5000/5 A g^{-1}**
	SAG//LFP	1.0-4.6	202-180 151-121 86-44	0.78-1.54 2.97-5.66 10.5-18.2	65%/1000/5 A g^{-1} 64%/2000/5 A g^{-1} 64%/3000/5 A g^{-1} 60%/4000/5 A g^{-1} 50%/5000/5 A g^{-1}
Li-DIBs	**NTO//KS6**	**0.01-5.3**	**311-278** **262-234** **162**	**0.8-2.2** **4.5-9.4** **18.6**	**82%/100/2 A g^{-1}** **72%/200/2 A g^{-1}** **65%/300/2 A g^{-1}** **60%/400/2 A g^{-1}** **57%/500/2 A g^{-1}**
	SAG//KS6	0.01-5.3	292-232 167-130 48	0.45-1.3 2.86-8.42 14.4	46%/100/2 A g^{-1} 28%/200/2 A g^{-1}

Table S5. A comparison for the performance of the NTO//AC LICs in the study with some reported LICs.

LICs	Working voltage / V	Energy density / Wh kg^{-1}	Power density / kW kg^{-1}	Cycling behavior / retention%, repeated cycles, current density	Refs.
T-Nb_2O_5/Graphene paper//AC	0.5-3.0	47-15	0.39-18	93% /2000/ 0.25 A g^{-1}	5
$LiNi_{0.5}Mn_{1.5}O_4$//AC	1.5-3.25	19-8	0.13-3.5	81% /3000/ 1 A g^{-1}	6
$TiNb_2O_7$@C//CFs	0.8-3.2	110.4-20	0.1-5.46	77% /1500/ 0.2 A g^{-1}	7
SnO_2-C//C	0.5-4.0	110-45	0.19-2.96	80% /2000/ 1 A g^{-1}	8
Fe_2O_3@C//N-HPC	1.0-4.0	65-31	0.368-9.2	84% /1000/ 1 A g^{-1}	9
TiO_2@EEG//EEG	0.0-3.0	72-10	0.303-2.0	68% /1000/ 1.5 A g^{-1}	10
Some recently reported LICs based on perovskite anodes					
$KNi_{0.1}Co_{0.9}F_3$//AC	0-4.5	96-11	0.33-10.5	64% /1000/ 5 A g^{-1}	11
$Na_{0.85}Ni_{0.45}Co_{0.55}F_{3.56}$//AC	0-4.3	96.1-33.4	0.5-17.2	68% /1000/ 5 A g^{-1}	12
$KCo_{0.54}Mn_{0.46}F_3$/rGO//AC	0-4.4	87.7-24.8	0.5-7.4	65% /2000/ 5 A g^{-1}	13
$NaTaO_3$//AC	**0.01-4.5**	**88.4 75.5 69.1 61.1 52.2 43.4**	**0.7 1.1 2.3 4.5 8.9 18.2**	**80% /1000/ 5 A g^{-1} 76% /1500/ 5 A g^{-1} 72% /2000/ 5 A g^{-1}**	**This work**

Table S6. A comparison for the performance of the NTO//LFP LIBs in the study with some reported LIBs.

LIBs	Working voltage / V	Energy density / Wh kg^{-1}	Power density / kW kg^{-1}	Cycling behavior / retention%, repeated cycles, current density	Refs.
SLA1025 graphite//LCO	2.5-4.2	136	1.15		14
Graphene/Si multilayer// $LiNi_{1/3}Mn_{1/3}Co_{1/3}O_2$	3-4.3	156	0.03	70.4%/15/0.0375 A g^{-1}	15
TiO_2 nanofiber//LMO	1.7-2.5	220	0.314	90%/700/0.3 A g^{-1}	16
TiO_2 hollow nanofiber//LFP	0.9-2.5	165	0.16	88%/300/0.1 A g^{-1}	17
LTO//$LiNi_xCo_yMn_{1-x-y}O_2$	1.5-2.7	90	2.2		18
FeSb-TiC//LNMO	2.0-5.0	260	0.127	68%/50/0.0365 A g^{-1}	19
$Li_4Ti_5O_{12}$-$Li_2Ti_3O_7$// LFP	1.9-2.5	75	0.048		20
TiO_2(B) nanowires//$LiNi_{0.5}Mn_{1.5}O_4$	2.0-3.5	150	0.132	89%/100/0.5 C	21
Ni_3N nanosheets//LNMO	2.5-3.9	120	3.39	99%/250/1.4 A g^{-1}	22
Sn-C// $Li[Ni_{0.45}Co_{0.1}Mn_{1.45}O_4]$	3.1-4.8	170	0.18		23
Some recently reported perovskite anodes					
$KNi_{0.1}Co_{0.9}F_3$//LFP	0-4.7	173-29	0.75-15.3	67% /2000/ 2 A g^{-1}	11
$Na_{0.85}Ni_{0.45}Co_{0.55}F_{3.56}$//LFP	1-4.7	196.2-35.2	0.8-19.2	63% /2000/ 3 A g^{-1}	12
$KCo_{0.54}Mn_{0.46}F_3$/rGO//LFP	0-4.7	307.6-68.6	0.6-12.4	52% /5000/ 5 A g^{-1}	13
NTO//LFP	**0.01-4.5**	**205** **182** **151** **119** **92** **70**	**0.9** **1.7** **3.3** **6.3** **12.3** **24.1**	**80%/1000/5 A g^{-1}** **71%/2000/5 A g^{-1}** **67%/3000/5 A g^{-1}** **63%/4000/5 A g^{-1}** **60%/5000/5 A g^{-1}**	**This work**

Table S7. A comparison for the performance of the NTO//KS6 Li-DIBs in the study with some reported Li-DIBs.

Li-DIBs	Working voltage / V	Energy density / Wh kg^{-1}	Power density / kW kg^{-1}	Cycling behavior / retention%, repeated cycles, current density	Refs.
Graphite//Graphite	0.01-5.2	108		67%/50/0.05 A g^{-1}	24
Si-compound//Graphite	0-3	54		53%/100/0.1 A g^{-1}	25
Nb_2O_5//Graphite	1.5-3.5	52		84%/100/0.1 A g^{-1}	26
Li//Graphite	3.4-5.0	220		71%/500/0.05 A g^{-1}	27
TiO_2//Graphite	1.5-3.7	36		88%/50/0.1 A g^{-1}	28
MoO_3//KS6	1.5-3.5	77		90%/200/0.081 A g^{-1}	29
AC// Graphite	0-3.5	150		98% /100 /1.86 mA cm^{-2}	30
Graphite//Graphite	3-5	170		94%/500/0.5 A g^{-1}	31
Al//Graphite	3.0-5.0	150	1.2	98%/600/0.2 A g^{-1}	32
Graphite(MTI)//KS6	3.0-5.1	125	0.4	90%/200/0.5 A g^{-1}	33
RGO//Graphite	0-4.0	70	1.33	74%/50/1.33 A g^{-1}	34
Some recently reported perovskite anodes					
$NaNbO_3$//KS6	0.01-5.4	329-60	0.74-13.4	71%/100/2 A g^{-1}	4
$KNi_{0.1}Co_{0.9}F_3$//918	0.5-5.2	152-46	0.9-10.4	74%/300/2 A g^{-1}	11
$Na_{0.85}Ni_{0.45}Co_{0.55}F_{3.56}$//KS6	0.01-5.0	155.1-7.9	0.6-20.4	53%/300/2 A g^{-1}	12
NTO//KS6	**0.01-5.3**	**311** **278** **262** **234** **162**	**0.8** **2.2** **4.5** **9.4** **18.6**	**82%/100/2 A g^{-1}** **72%/200/2 A g^{-1}** **65%/300/2 A g^{-1}** **60%/400/2 A g^{-1}** **57%/500/2 A g^{-1}**	**This work**

Table S8. Performance summary of the NTO//AC LICs in the study under low (-20^{o}C) and high (40^{o}C) temperatures.

Capacitor system	T / ℃	Working voltage / V	Energy density / Wh kg^{-1}	Power density / kW kg^{-1}	Cycling behavior / retention%, repeated cycles, current density
NTO//AC	-20	0.01-4.5	26.2-20.8 14.4-10.8 6.8	0.56-1.1 2.3-4.5 9.0	71%/500/1 A g^{-1} 61%/1000/1 A g^{-1}
	40	0.01-4.5	90.5-71.9 64.4-58.8 50	0.6-1.1 2.3-4.6 8.6	72%/500/2 A g^{-1} 53%/1000/2 A g^{-1}

Table S9. Performance summary of the NTO//LFP LIBs in the study under low (-20°C) and high (40°C) temperatures.

Capacitor system	T / ℃	Working voltage / V	Energy density / Wh kg^{-1}	Power density / kW kg^{-1}	Cycling behavior / retention%, repeated cycles, current density
NTO//LFP	-20	0.01-4.5	42.6-25.3 16.0-10.1 5.3	0.8-1.5 3.0-5.7 11.2	92%/5000/1 A g^{-1}
	40	0.01-4.5	251.0-238.0 213.3-176.2 131.0	0.84-1.68 3.31-6.54 12.4	60%/500/2 A g^{-1} 50%/2000/2 A g^{-1}

Table S10. Performance summary of the NTO//KS6 Li-DIBs in the study under low (-20^{o}C) and high (40^{o}C) temperatures.

Capacitor system	T / ℃	Working voltage / V	Energy density / Wh kg^{-1}	Power density / kW kg^{-1}	Cycling behavior / retention%, repeated cycles, current density
NTO//KS6	-20	0.01-5.3	210.4-94.8 74.0-40.8 18	0.56-1.3 3.8-7.2 12.0	90%/200/1 A g^{-1} 81%/500/1 A g^{-1} 80%/1000/1 A g^{-1} 64%/3000/1 A g^{-1}
	40	0.01-5.3	345-256 194-81 20	1.13-2.24 4.72-8.60 12.0	62%/100/2 A g^{-1}

References

1. Y. He, Y. F. Zhu and N. Z. Wu, *J. Solid State Chem.*, 2004, **177**, 3868-3872.
2. C.-C. Hu and H. Teng, *Appl. Catal. A: Gen.*, 2007, **331**, 44-50.
3. X. Li and J. L. Zang, *J. Phys. Chem. C*, 2009, **113**, 19411-19418.
4. T. Yan, R. Ding, D. F. Ying, Y. F. Huang, Y. X. Huang, C. N. Tan, X. J. Sun, P. Gao and E. H. Liu, *J. Mater. Chem. A*, 2019, **7**, 22884-22888.
5. L. P. Kong, C. F. Zhang, J. T. Wang, W. M. Qiao, L. C. Ling and D. H. Long, *ACS Nano*, 2015, **9**, 11200-11208.
6. N. Arun, A. Jain, V. Aravindan, S. Jayaraman, W. Chui Ling, M. P. Srinivasan and S. Madhavi, *Nano Energy*, 2015, **12**, 69-75.
7. X. F. Wang and G. Z. Shen, *Nano Energy*, 2015, **15**, 104-115.
8. W.-H. Qu, F. Han, A.-H. Lu, C. Xing, M. Qiao and W. -C. Li, *J. Mater. Chem. A*, 2014, **2**, 6549-6557.
9. X. L. Yu, J. J. Deng, C. Z. Zhan, R. T. Lv, Z.-H. Huang and F. Y. Kang, *Electrochim. Acta*, 2017, **228**, 76-81.
10. F. X. Wang, C. Wang, Y. J. Zhao, Z. C. Liu, Z. Chang, L. J. Fu, Y. S. Zhu, Y. P. Wu and D. Y. Zhao, *Small*, 2016, **12**, 6207-6213.
11. Q. L. Xu, R. Ding, W. Shi, D. F. Ying, Y. F. Huang, T. Yan, P. Gao, X. J. Sun and E. H. Liu, *J. Mater. Chem. A*, 2019, **7**, 8315-8326.
12. W. Shi, R. Ding, Q. L. Xu, T. Yan, Y. X. Huang, C. N. Tan, X. J. Sun, P. Gao and E. H. Liu, *Chem. Commun.*, 2019, **55**, 6739-6742.
13. D. F. Ying, R. Ding, Y. F. Huang, W. Shi, Q. L. Xu, C. N. Tan, X. J. Sun, P. Gao and E. H. Liu, *J. Mater. Chem. A*, 2019, **7**, 18257-18266.
14. V. G. Khomenko, V. Z. Barsukov, J. E. Doninger and I. V. Barsukov, *J. Power Sources*, 2007, **165**, 598-608.
15. L. Ji, H. Zheng, A. Ismach, Z. Tan, S. Xun, E. Lin, V. Battaglia, V. Srinivasan and Y. Zhang, *Nano Energy*, 2012, **1**, 164-171.
16. V. Aravindan, J. Sundaramurthy, P. S. Kumar, N. Shubha, W. C. Ling, S. Ramakrishna and S. Madhavi, *Nanoscale*, 2013, **5**, 10636-10645.
17. X. Zhang, V. Aravindan, P. S. Kumar, H. Liu, J. Sundaramurthy, S. Ramakrishna and S. Madhavi, *Nanoscale*, 2013, **5**, 5973-5980.
18. N. Takami, H. Inagaki, Y. Tatebayashi, H. Saruwatari, K. Honda and S. Egusa, *J. Power Sources*, 2013, **244**, 469-475.
19. Z. Moorhead-Rosenberg, E. Allcorn and A. Manthiram, *Chem. Mater.*, 2014, **26**, 5905-5913.
20. G.-N. Zhu, L. Chen, Y.-G. Wang, C.-X. Wang, R.-C. Che and Y.-Y. Xia, *Adv. Funct. Mater.*, 2013, **23**, 640-647.
21. G. Armstrong, A. R. Armstrong, P. G. Bruce, P. Reale and B. Scrosati, *Adv. Mater.*, 2006, **18**, 2597-2600.
22. M.-S. Balogun, Y. Zeng, W. Qiu, Y. Luo, A. Onasanya, T. K. Olaniyi and Y. Tong, *J. Mater. Chem. A*, 2016, **4**, 9844-9849.
23. J. Hassoun, K.-S. Lee, Y.-K. Sun and B. Scrosati, *J. Am. Chem. Soc.*, 2011, **133**, 3139-3143.

24. J. A. Read, A. V. Cresce, M. H. Ervin and K. Xu, *Energy Environ. Sci.*, 2014, **7**, 617-620.
25. H. Nakano, Y. Sugiyama, T. Morishita, M. J. S. Spencer, I. K. Snook, Y. Kumai and H. Okamoto, *J. Mate. Chem. A*, 2014, **2**, 7588-7592.
26. G. Park, N. Gunawardhana, C. Lee, S.-M. Lee, Y.-S. Lee and M. Yoshio, *J. Power Sources*, 2013, **236**, 145-150.
27. P. Meister, V. Siozios, J. Reiter, S. Klamor, S. Rothermel, O. Fromm, H.-W. Meyer, M. Winter and T. Placke, *Electrochim. Acta*, 2014, **130**, 625-633.
28. A. K. Thapa, G. Park, H. Nakamura, T. Ishihara, N. Moriyama, T. Kawamura, H. Y. Wang and M. Yoshio, *Electrochim. Acta*, 2010, **55**, 7305-7309.
29. N. Gunawardhana, G.-J. Park, N. Dimov, A. K. Thapa, H. Nakamura, H. Y. Wang, T. Ishihara and M. Yoshio, *J. Power Sources*, 2011, **196**, 7886-7890.
30. T. Ishihara, Y. Yokoyama, F. Kozono and H. Hayashi, *J. Power Sources*, 2011, **196**, 6956-6959.
31. S. Rothermel, P. Meister, G. Schmuelling, O. Fromm, H.-W. Meyer, S. Nowak, M. Winter and T. Placke, *Energy Environ. Sci.*, 2014, **7**, 3412-3423.
32. X. L. Zhang, Y. B. Tang, F. Zhang and C.-S. Lee, *Adv. Energy Mater.*, 2016, **6**, 1502588.
33. C. Y. Chan, P.-K. Lee, Z. Xu and D. Y. W. Yu, *Electrochim. Acta*, 2018, **263**, 34-39.
34. X. Y. Shi, W. Zhang, J. F. Wang, W. T. Zheng, K. K. Huang, H. B. Zhang, S. H. Feng, H. Chen, *Adv. Energy Mater.* 2016, ***6***, 1601378.